공학박사 학위논문

Improvement in Long-term Stability of Capacitive Deionization by Polymer Coating on Carbon Electrode

고분자 코팅 전극을 이용한 축전식 탈염 공정의 장기 운전 내구성 향상

2020년 2월

서울대학교 대학원

화학생물공학부

조 규 식

Improvement in Long-term Stability of Capacitive Deionization by Polymer Coating on Carbon Electrode

by

Kyusik Jo

Under the supervision of

Professor Changha Lee, Ph. D.

A dissertation submitted in partial fulfillment of

the requirements for the Degree of

Doctor of Philosophy

February 2020

SCHOOL OF CHEMICAL AND BIOLOGICAL

ENGINEERING

SEOUL NATIONAL UNIVERSITY

Abstract

Capacitive deionization (CDI) is one of state-of-art technology for desalination of brackish water to supply enough water for day life. CDI has attracted attention as an efficient desalination technology in terms of energy consumption, water recovery, and environment-friendliness compared to the other desalination technology. However, CDI suffers from desalination performance degradation in long-term operation, which is critical issue for practical application. The degradation could be overcome by inhibiting the carbon oxidation, which is the main reason for degradation, but there were little research focusing on the inhibition of carbon oxidation.

This dissertation aimed to provide a guideline for improving long-term stability of CDI by evaluating long-term stability of CDI and polymer-coated CDI and by investigating the working mechanisms for how polymer affects to transportation phenomena or electrical properties of the electrode. First, the salt adsorption capacity (SAC) changes of CDI using the electrode, that polydopamine (PDA) or ion exchange polymer (IEP) was coated on without the polymer layer on outer surface of the electrode, was traced. As a result, long term stability of polymer-coated CDI was improved by inhibiting carbon oxidation reactions due to the coverage of activated carbon surface by PDA

and IEP without any additional polymer layer on outer surface of the electrode. PDA coating prevented the carbon oxidation reaction from occurring as much as 10% and IEP coating was more effective than PDA, resulting in approximately 80% higher long-term stability. It was because the thicker coating layer than PDA coating inhibits carbon oxidation more successfully.

Second, to determine the role of IEP layer, the pre-oxidized electrode was tested in CDI and MCDI and the long-term stability of CDI using IEP-coated electrodes coated with various thicknesses (30 μm, 100 μm) were measured and compared. As major result, MCDI with pre-oxidized electrode for 24 h showed less performance reduction compared to the case of CDI. It means that ion exchange membrane has an effect on compensating the influence of carbon oxidation. This effect was investigated systemically by IEP coating with different thickness. CDI using the electrode with thicker IEP layer showed better long-term stability represented by less SAC reduction. Therefore, it can be concluded that IEP layer on outer surface of electrode also appeared to play a role as the compensation barrier that utilizes repulsed co-ions by positive PZC shift that formation of IEP layer as well as a role that inhibits the carbon oxidation more based on larger charge transfer resistance.

Therefore, it was found that the stability of CDI can be further improved by coating activated carbon using various polymers and forming an IEP layer

having an appropriate thickness. This research is meaningful in that it suggests a big direction to improve the stability required for the industrial application of CDI.

Keywords: Capacitive deionization, Long-term stability, PDA coating, Ion exchange polymer coating, Carbon oxidation, Potential of zero charge shift

Student number: 2014-31081

Table of contents

Abstract ····· I

1. Introduction ····· 1

1.1. Research background ····· 1

1.2. Objective ····· 3

2. Literature review ····· 5

2.1. Introduction of CDI ····· 5

2.2. Stability of CDI ····· 12

2.2.1. Performance degradations in CDI 12

2.2.2. Faradaic reactions as side reactions in CDI 14

2.2.3. Carbon oxidation at positive electrode 15

2.2.4. Attempts to improve long-term stability 28

2.2.5. Stability of MCDI 29

2.3. Polymer-coated electrode for CDI ····· 35

2.3.1. Polydopamine coating 35

2.3.2. Polyaniline coating 39

2.3.3. Ion-exchange polymer coating 39

2.4. Limitations of previous studies ····· 42

3. Long term stability of CDI with polymer-coated electrode ····· 45

3.1. Backgrounds ····· 45

3.2. Materials and method ····· 48

3.2.1. Electrode fabrication 48

3.2.2. Polymer coating 48

3.2.3. Electrode characterization 49

3.2.4. Desalination test 50

3.2.5. Anode replacing long-term operation 53

3.3. Results and discussion ····· 53

3.3.1. Anode replacing long-term operation 53

3.3.2. Polydopamine coating 60

3.3.3. Ion-exchange polymer coating 70

3.4. Summary ····· 76

4. Effect of IEP layer thickness on long term stability ····· 77

4.1. Background ····· 77

4.2. Materials and method ····· 77

4.2.1. Pre-oxidation of carbon electrode.....77

4.2.2. Preparation of IEP-coated electrode 81

4.2.3. Electrode characterization.....81

4.3. Results and Discussion ····· 83

4.3.1. MCDI test using pre-oxidized electrode.....83

4.3.2. Long-term operation of IEP-CCDI with different thickness 93

5. Conclusion ····· 106

References····· 108

국문 초록 ····· 126

List of figures

Figure 2-1 Working principle of capacitive deionization (CDI)····· 6

Figure 2-2 Various capacitive deionization (CDI) architectures (Suss et al., 2015)····· 10

Figure 2-3 Results showing degradation in desalination performance reported by (a) Bouhadana et al., 2011, (b) Omosebi et al., 2014, and (c) Gao et al., 2014.····· 13

Figure 2-4 SEM images with carbon (red dots) and oxygen (green dots) mapping by EDAX of activated carbon cloth (ACC) electrodes before and after long term operation with a flow-by cell. (A) A pristine ACC electrode, (B) The negatively polarized ACC electrode after long term experiment, (C) The positively polarized ACC electrode after long term experiment (Cohen et al., 2015).····· 17

Figure 2-5 Effluent NaCl concentration in ppm vs. time in day measured during prolonged cycling. The four plots relate to selected time domains. During charge and discharge step, 0.9 V and 0 V were applied, respectively (Cohen et al., 2015). ····· 18

Figure 2-6 Effluent NaCl concentration in ppm vs. time in day measured during prolonged cycling using N_2-purged influent. The four plots relate to selected time domains. During charge and discharge step, 0.9 V and 0 V were

applied, respectively (Cohen et al., 2015). ····· 21

Figure 2-7 (a) Conductivity profile at first 3 cycles and last 3 cycles and (b) normalized salt adsorption capacity (SAC) of CDI, MCDI, and CDI with N_2 purging. ····· 22

Figure 2-8 Schematic diagram for carbon oxidation and formation of oxygen functional groups (Yi et al., 2017) ····· 24

Figure 2-9 Schematic diagram for the effect of anode PZC shift. (a) Initial state, (b) first step: reduction of salt adsorption capacity (SAC) (shifted under 0.6 V), (c) second step: observation of inversion peak (shifted at 0.6 V), (d) third step: fully inversed (shifted over 1.2 V), and (e) fourth step: further SAC increase of inversed CDI (shifted over 1.2 V). ····· 27

Figure 2-10 (a) Effluent conductivity profile of CDI and MCDI after 6 h operation and (b) that after 35 h operation. (c) Charge efficiency changes during 50 h operation (Omosebi et al., 2014). ····· 33

Figure 2-11 (a) Schematic diagram explaining the consumption of charges applied during charging step in CDI, and (b) in MCDI. (c) The conductivity profile of CDI and MCDI and (d) salt adsorption capacity (SAC) changes of CDI and MCDI (Yu et al., 2018). ····· 34

Figure 2-12 (a) Polydopamine (PDA) as a component of bioinspired adhesive plaque (Lee et al., 2007), (b) polymerization mechanism of

dopamine (Xie et al., 2017)····· 37

Figure 2-13 Conductivity changes of CDI using polydopamine (PDA)-coated activated carbon as an electrode material (Xie et al., 2017)····· 38

Figure 2-14 (a) Cross section SEM image of pristine AC electrode and (b) that of ion-exchange polymer (IEP)-coated electrode. Comparison result of (c) salt removal efficiency (equal to SAC in this thesis) and (d) current efficiency (equal to charge efficiency in this thesis) (Kim and Choi, 2010c). ····· 41

Figure 3-1 Schematic diagram of the effect of polymer coating on carbon electrode. ····· 47

Figure 3-2 Schematic diagram for desalination test setup. ····· 52

Figure 3-3 Conductivity change in anode-changing long term operation ····· 55

Figure 3-4 (a) Cyclic voltammetry (CV) profile, (b) enlarged oxidation current and reduction current showing potential of zero charge (PZC), (c) PZC changes by repeated cycles, and (d) changes of salt adsorption capacity (SAC) and SAC reduction versus PZC ····· 59

Figure 3-5 Contact angle image (a) before and (b) after PDA modification····· 61

Figure 3-6 Cross section SEM images of polydopamine (PDA)–coated electrode with (a) 1000 and (c) 3000 magnifications and that of pristine electrode with (b)1000 and (d) 3000 magnifications ····· 62

Figure 3-7 Normalized conductivity during long-term operation of (a) PDA-CDI and (b) CDI without coating····· 64

Figure 3-8 Comparison of normalized salt adsorption capacity (SAC) changes before and after polydopamine (PDA) modification ····· 65

Figure 3-9 Cyclic voltammetry result of (a) PDA-CDI and (b) CDI before and after long-term operation ····· 69

Figure 3-10 (a) Changes in conductivity profiles and (b) salt adsorption capacity (SAC) of CDI and PC–CDI during 150 cycles of operation. (c) Enlarged conductivity profile at early cycles and (d) that at later cycles. ·· 71

Figure 3-11 Cyclic voltammetry of (a) PC-electrode and (b) Anode potential changes for 150 cycles. ····· 73

Figure 3-12 Cross section view of PC–CDI electrode with (a) 1000 magnification and (b) 3000 magnification.····· 75

Figure 4-1 Schematic diagram for pre-oxidation of carbon electrode · 80

Figure 4-2 (a) Effluent conductivity profile of pre-oxidized electrode at initial cycle and after 24 h operation and (b) long-term operated electrode

during 50 h ····· 84

Figure 4-3 (a) Normalized conductivity profiles of 4 CDI assemblies, (b) that of 4 MCDI assemblies, and (c) relative SACs of CDI and MCDI based on the cell using both pristine electrode ····· 89

Figure 4-4 Schematic diagram about the effect of PZC shift to ion adsorption when oxidized electrode was used as (a) an anode and (b) a cathode. ····· 91

Figure 4-5 Schematic diagram for explaining the mechanisms of desalination performance improvement in MCDI compared to the performance in CDI ····· 92

Figure 4-6 SEM images of (a) IEP–CCDI30 and (b) IEP–CCDI100 ·· 96

Figure 4-7 (a) Salt adsorption capacity (SAC) changes of thickness-controlled CCDI and CDI for 150 cycles and (b) the relationship between IEP-layer thickness and SAC, SAC reduction. ····· 97

Figure 4-8 Cyclic voltammetry profile of (a) IEP–CCDI30 and (b) IEP–CCDI100 before and after long-term operation. ····· 98

Figure 4-9 (a) Charge efficiency and (b) Nyquist plot of pristine and three IEP-coated electrodes with variation in thickness. An inset figure in (b) is enlarged impedance profile at high frequency range. ····· 101

Figure 4-10 Charge efficiency of CDI, PC–CDI, IEP–CCDI30, and IEP–

CCDI100. ····· 104

List of tables

Table 4-1 SAC values of CDI and MCDI for four pairs using pristine and pre-oxidized electrode ····· 90

Table 4-2 SAC changes and resistances of pristine CDI and IEP-coated CDI ····· 102

1. Introduction

1.1. Research background

Capacitive deionization (CDI) is one of state-of-art technology for desalination of brackish water. CDI has attracted attention as an efficient desalination technology in terms of energy consumption, water recovery, and environment-friendliness compared to the other desalination technology (Suss et al., 2015). The principle of CDI is that ionic species in the water are attracted to the when potential was applied and form electrical double layer (EDL) during desalinated water continuously flows out. Therefore, it has been reported that CDI has advantages in energy and sustainability because well-known problems in membrane desalination such as high pressure and chemical usage were less critical in CDI (Suss et al., 2015). Furthermore, the advantages of CDI have been enhanced by the application of ion exchange membrane (IEM) in front of each carbon electrode (referred as MCDI) (Kim and Choi, 2010a,Lee et al., 2011) to prevent co-ion repulsion which induces dissipation of charges (Zhao et al., 2009). These efforts led to the improvement in charge efficiency from 50% to up to 90% (Biesheuvel et al., 2011,Hassanvand et al., 2017,Kim and Choi, 2010b,Omosebi et al., 2014) and in the salt adsorption capacity (SAC) (Biesheuvel et al., 2011,Lee et al., 2006,Li et al., 2011,Liu et al., 2014).

The high charge efficiency and SAC of the MCDI is due to the fact that

the IEM acts as a charge barrier, so that no charge is wasted in order to remove co-ions from the electrode. However, the IEM used in MCDI are products used in the electrodialysis (ED), and have disadvantages of being thick and expensive. To overcome these disadvantages in perspective of the modification of IEM, the thickness, physical strength, ion exchange capacity, and transport number must be improved. However, these characteristics are trade-offs, and thus there is a limitation in improving the IEM.

To overcome the limitation, studies have been conducted to form a charge barrier by coating an ion exchange polymer (IEP) on a carbon electrode with lower thickness (Asquith et al., 2014,2015,Kim and Choi, 2010a,Kim and Choi, 2010b,Kim and Choi, 2010c). Literatures have reported that the IEP coating improved SAC, suggesting the successful replacement of MCDI's IEM based on the increase in charge efficiency due to the role as a charge barrier. In addition, studies have shown that the IEP that are selective to specific ions can be used to provide the corresponding ion selectivity to CDI (Kim et al., 2013,Kim and Choi, 2012,Yeo and Choi, 2013).

In spite of the increase in SAC and charge efficiency, studies about evaluation or improvement of long-term operation stability of CDI coated with IEPs are insufficient. First of all, in the case of CDI without IEP, SAC reduction of approximately 90% or more has been reported in long term

operation (Bouhadana et al., 2011a,Cohen et al., 2013,Yu et al., 2018). The reason for the SAC reduction is the change in surface properties due to carbon oxidation (Avraham et al., 2010). When the potential is applied in CDI, various side reactions occur (Kim et al., 2016,Lee et al., 2010). Among them, carbon reacts with water molecules to form oxygen functional groups which have negative charges on the anode surface (Bouhadana et al., 2011b,Omosebi et al., 2014). Then, the surface charge of the oxidation electrode, represented by potential of zero charge (PZC), is shifted in the positive direction, and the desalting capacity is reduced due to the imbalance of ion adsorption behavior between the anode and cathode. On the other hand, high stability of MCDI was reported compared to the stability of CDI (Yu et al., 2018). In that paper, the reasons were the smaller cathodic side reactions and the lower PZC shift of the anode because of the existence of IEM. However, the mechanisms of the high stability of MCDI was little investigated with focus on the role of IEM.

1.2. Objective

To contribute the practical application of CDI, this dissertation aimed to provide a guideline for improving long-term stability of CDI by evaluating long-term stability of CDI and polymer-coated CDI and by investigating the working mechanisms for how polymer affects to transportation phenomena

or electrical properties of the electrode.

For those purpose, first, the influence of carbon oxidation was determined by changing only anode periodically without changing the cathode. After that, polydopamine (PDA) or IEP was coated on the activated carbon electrode and its long-term stability was evaluated. To analyze the reason for the measured long-term stability, electrochemical analyses were implemented.

Second, to determine the role of IEP layer, IEP layer thickness were set as a major variable and SAC changes were traced. This determination is expected to be able to define the role of IEP before and after the carbon oxidation.

From these approaches, it is expected that many researchers or technicians who want to improve the long-term stability of CDI get some guideline or inspirations. And finally, it is expected that CDI will be applied to broad areas where deionized water is necessary.

2. Literature review

2.1. Introduction of CDI

CDI is one of the successful convergence technologies in which the principle of supercapacitors, which is an electrical energy storage devices, is applied to desalination, an environmental technology (Yoon et al., 2019). The principle of CDI is to apply the potential to the electrode while passing water between the pair of electrodes as shown in Figure 2-1. After that, the two electrodes are short-circuited or reversed to regenerate to their initial state, and the desalination and regeneration are operated alternately to produce treated water continuously. This technology uses electric force, which does not require a high-pressure pump, and because of the low pressure drop, less fouling is considered to be more environmentally friendly and safer than conventional desalination technology (Suss et al., 2015). It is also based on the principle of energy storage technology and because energy is stored in the desalination process, it is possible to recover the energy while recovering the module (Álvarez-González et al., 2016,Dlugolecki and van der Wal, 2013,Kang et al., 2016,Ma et al., 2019b,Pernía et al., 2018).

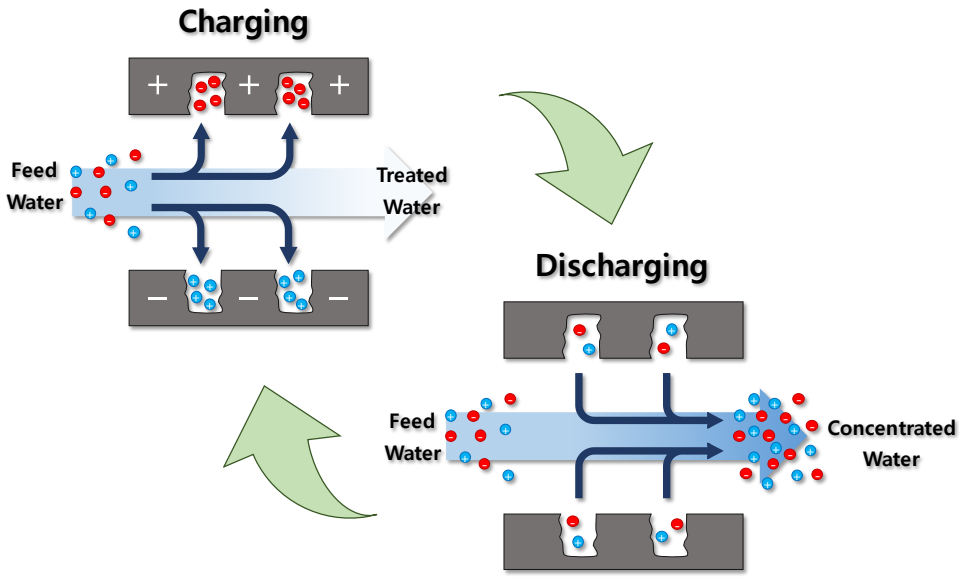

Figure 2-1 Working principle of capacitive deionization (CDI)

On the principle of operation, the capacitive deionization module is composed of a pair of electrodes, a flow path to help water flow, a current collector to apply an electric potential, and other auxiliary devices. Although these basic components can actually be used to desalination, several attempts have been conducted to achieve higher performance. The various forms of CDI that have been developed so far are summarized in Figure 2-2 (Suss et al., 2015) as a result of attempts. First, flow-by CDI (Figure 2-2(a)) and flow-through CDI (Figure 2-2(b)) are divided according to how the flow path is formed. In the case of flow-by CDI, water does not flow directly into the electrode, but a porous spacer inserted between the electrode and the electrode serves as a flow path where water flows and an insulator that prevents the electrode from shorting, simultaneously. On the other hand, in the flow-through CDI, since water flows through the electrode directly and sequentially, electrodes serve as a flow path. Therefore, the advantage of flow-through CDI is that the electrode pores could be utilized almost fully, but the disadvantage is that large pores of the electrode are essentially required unlike the flow-by CDI (Suss et al., 2012).

Next, systems that aimed to improve desalination performance by adding or replacing components in CDI are shown in Figure 2-2(C), (E), and (F). Figure 2-2(c) shows the membrane CDI (MCDI) with an ion exchange

membrane inserted in front of the electrode. MCDI is a system with improved energy and charge efficiency by reducing charge dissipation which occur in conventional CDI. On the other hand, the system that replaces the electrode material of CDI, which is mainly carbon material, with the material used in the rechargeable battery is the desalination battery in Figure 2-2(F). hybrid CDI shown in Figure 2-2(E) is the converged system developed to complement the cost issues in desalination battery by replacing expensive silver electrode to activated carbon electrode. Desalination batteries and hybrid CDIs are reported to have very high performance compared to various CDI systems using carbon materials (Choi et al., 2018,Lee et al., 2014).

The various CDI systems mentioned so far basically use electrodes fixed to the current collector. In this case, a certain amount of wastewater is required to regenerate a full capacity module. In other words, deionized water is produced during the desalination by applying a potential, but the deionized water cannot be produced when the desalination is completed and the module is regenerated. Therefore, a single module cannot produce treated water continuously. The system that solved these shortcomings through the conversion of ideas is the flow-electrode CDI (FCDI) shown in Figure 2-2(G) ~ (I). FCDI uses a slurry type electrode with a certain amount of carbon material dispersed in water. The clean electrode with no ions adsorbed is

continuously supplied to the module, and the electrode with ions adsorbed flows out of the module. Therefore, only water from which ions have been removed is continuously produced (Jeon et al., 2013) (Jeon et al., 2013). Electrodes that adsorb ions are regenerated through a separate system outside the module, and various techniques have been studied to effectively regenerate the electrodes (Jeon et al., 2014).

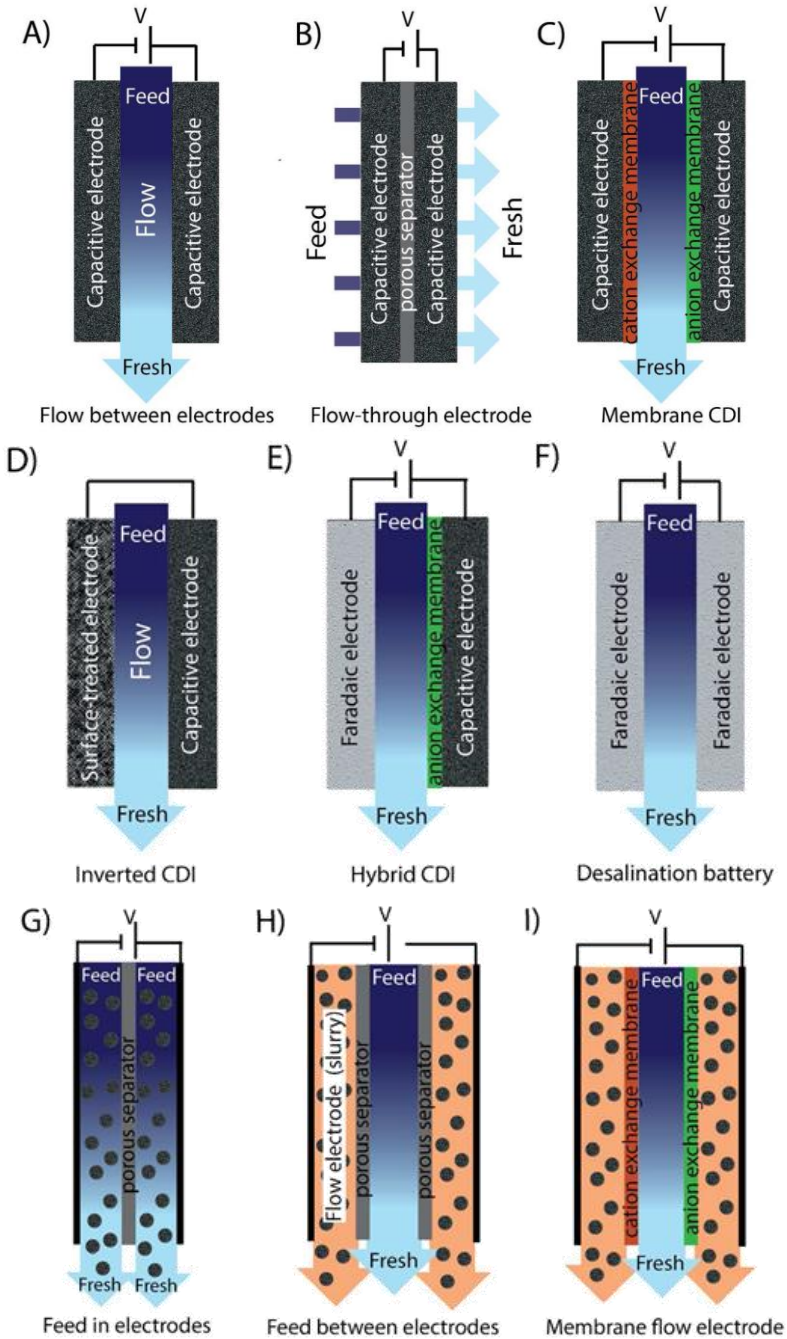

Figure 2-2 Various capacitive deionization (CDI) architectures (Suss et al., 2015)

Capacitive desalination processes are applied in various fields. Since the purpose of the capacitive deionization is to remove ions using electric force, the uncharged species are difficult to be removed, and only the charged species can be efficiently removed. However, this technique has yet to be limited for efficient influent concentration ranges due to the limited capacity of the electrode (Qin et al., 2019). Therefore, commercial CDI modules are currently applied to water with relatively low concentration such as groundwater, surface water, tap water treatment, and plant cooling water treatment. Nevertheless, CDI is compatible because its unique characteristic is that it can be given selectivity. There have been many reports to selectively remove nitrate (Kim et al., 2013,Kim and Choi, 2012,Yeo and Choi, 2013) or another anionic oxygen compounds (Bales et al., 2019,Kim et al., 2012a,Ma et al., 2019c,Tang et al., 2017b). As cation selective removal, hybrid CDI system have been applied (Lee et al., 2014,Yoon et al., 2018). In addition, pure manufacturability has been reported, which is essential for many electrical device manufacturing processes (Lee and Choi, 2012). Furthermore, the application as the novel water treatment converging advanced oxidation process and CDI is possible (Kim et al., 2015,Kim et al., 2018a,Kim et al., 2018b) to achieve desalination and oxidation (or disinfection) simultaneously.

2.2. Stability of CDI

2.2.1. Performance degradations in CDI

Despite the efficiency and differentiation of capacitive deionization, there are still obstacles to real application. As summarized in Figure 2-3, a significant reduction in performance was observed for long-term operation of a conventional CDI using carbon materials for at least 50 hours (Cohen et al., 2013,2015,Gao et al., 2014,Omosebi et al., 2014,Yu et al., 2018). In Figure 2-3 (a), the operation was performed for about 130 hours, and the decrease in performance and the inversion peak were observed. Inversion peak is a phenomenon in which ions are desorbed and adsorbed when 1.2V and 0V is applied, respectively, unlike the general phenomenon of adsorption at 1.2V and desorption at 0V. In Figure 2-3 (b) and (c), almost no ions are adsorbed after about 50 hours of desalination. For this reason, the most pointed out factor in the existing literature is the side reaction that occurs at the electrode when a potential of 1.2 V or higher is applied to CDI (Avraham et al., 2010,Bouhadana et al., 2011b).

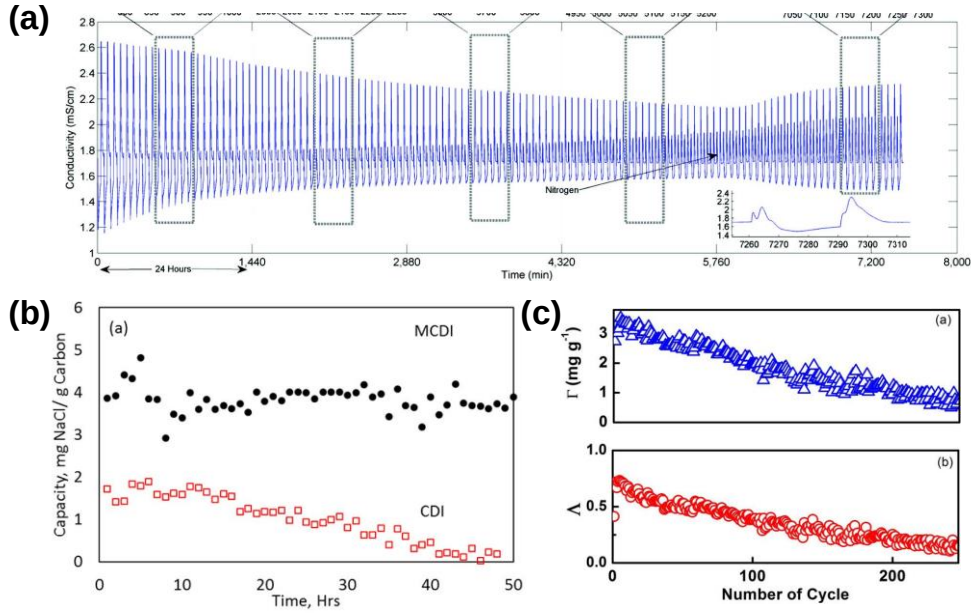

Figure 2-3 Results showing degradation in desalination performance reported by (a) Bouhadana et al., 2011, (b) Omosebi et al., 2014, and (c) Gao et al., 2014.

2.2.2. Faradaic reactions as side reactions in CDI

In CDI, various side reactions have been reported to occur at both the anode and the cathode (He et al., 2016,Tang et al., 2017a,Yu et al., 2018,Zhang et al., 2018). First, at the cathode, a reaction in which water molecules and dissolved oxygen react to generate hydrogen peroxide (Kim et al., 2016,Yu et al., 2018) and hydrogenation reaction of carbon are known (Zhang et al., 2018). Among the possible reactions in the general CDI applied 1.2V are as follows.

$$O_2 + 2H^+ + 2e^- \rightarrow H_2O_2 \qquad E = 0.28\ V \qquad \text{Rxn. (1)}$$

$$O_2 + 4H^+ + 4e^- \rightarrow 2H_2O \qquad E = 0.82\ V \qquad \text{Rxn. (2)}$$

As well expressed in the reaction equations (Rxn (1), (2)), dissolved oxygen is the main reactant and the product is hydrogen peroxide and water molecules. Since the reaction occurs in water, the formation of water molecules cannot be directly measured, but in the case of hydrogen peroxide, direct measurement is possible. As a result of the measurement, it was found that hydrogen peroxide was generated steadily throughout the charging step under 1.2V, and the generation of hydrogen peroxide occurred regardless of time even during long-term operation for 50 hours. However, the amount of charges consumed to the generation of hydrogen peroxide is relatively insignificant, accounting for about 10% of the total charges flowed in the deionization step (He et al., 2016,Kim et al., 2016,Tang et al., 2017a,Yu et al., 2018,Zhang

et al., 2018,Zhang et al., 2019).

On the other hand, oxidation of carbon, chlorine generation, and water decomposition can occur at the anode (Bouhadana et al., 2011b,He et al., 2016,Maass et al., 2008,Omosebi et al., 2014,Yu et al., 2018). Among these reactions, the following reactions is possible under CDI operating conditions (1.2 V). As can be seen in the reaction equations (Rxn (3)~(6)), the notable reaction is the formation of a negatively charged carboxylic functional group by the reaction between carbon and surface oxygen although there are the oxidation of carbon which may lead to carbon corrosion to dissolved carbon monoxide or carbon dioxide. The reason why the formation of negatively charged functional group is that CDI adsorbs ions by electrical attraction. That is, negatively charged surface can directly affect the adsorption characteristics sensitively because of the changes in surface charge on the electrode.

$$C + H_2O \rightarrow C - O_{ad} + 2H^+ + 2e^- \qquad E = -0.404\ V \qquad \text{Rxn. (3)}$$

$$C - O_{ad} + H_2O \rightarrow C - OO^- + 2H^+ + 2e^- \qquad E = 0.290\ V \qquad \text{Rxn. (4)}$$

$$C + H_2O \rightarrow CO + 2H^+ + 2e^- \qquad E = -0.093\ V \qquad \text{Rxn. (5)}$$

$$C + 2H_2O \rightarrow CO_2 + 4H^+ + 4e^- \qquad E = 0.090\ V \qquad \text{Rxn. (6)}$$

2.2.3. Carbon oxidation at positive electrode

The potential impact on CDI performance when the carbon surface is oxidized is degradation of the performance in long-term operation, as

mentioned in Section 2.2.1. The imbalance of the carbon surface charge of positive and negative electrode, represented by the PZC (PZC), mainly reported by the Kunlei Liu group (Gao et al., 2014) and the Doron Aurbach group (Cohen et al., 2013), affects performance degradation. In the long term operation, the PZC is gradually moved in the positive direction due to the carbon surface oxidation occurring at the anode (Cohen et al., 2015).

Figure 2-4 shows the results of EDS elemental analysis of surface oxidation during long term operation. When you look at the oxygen element analysis on the right side of the figure, you can see that it was increased after long-term operation (A<B<C), unlike the figure on the left (image) and center (carbon). Considering that A is the pristine, B is the cathode, and C is the Anode, the most oxygen found in C directly indicates that the anode is continuously oxidized, producing large amounts of oxygen functional groups. The paper has shown that the formation of these oxygen functional groups is directly related to the generation of inversion peaks and the reduction of desalination capacity (Figure 2-5). As shown in this figure, the inversion peak begins to be observed after about 0.9 days of operation at 0.9 V, and the effluent concentration changes significantly. The subsequent effluent concentration changes at 14 and 17 days show very similar conductivity profiles at the charge (0.9 V) and discharge (0 V) phases.

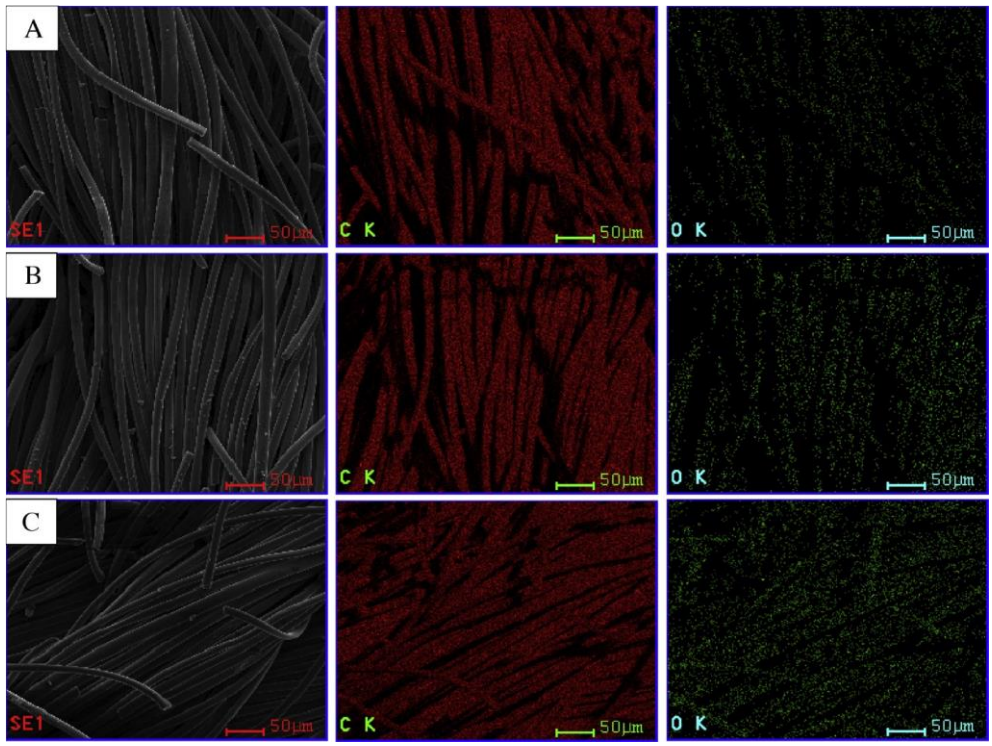

Figure 2-4 SEM images with carbon (red dots) and oxygen (green dots) mapping by EDAX of activated carbon cloth (ACC) electrodes before and after long term operation with a flow-by cell. (A) A pristine ACC electrode, (B) The negatively polarized ACC electrode after long term experiment, (C) The positively polarized ACC electrode after long term experiment (Cohen et al., 2015).

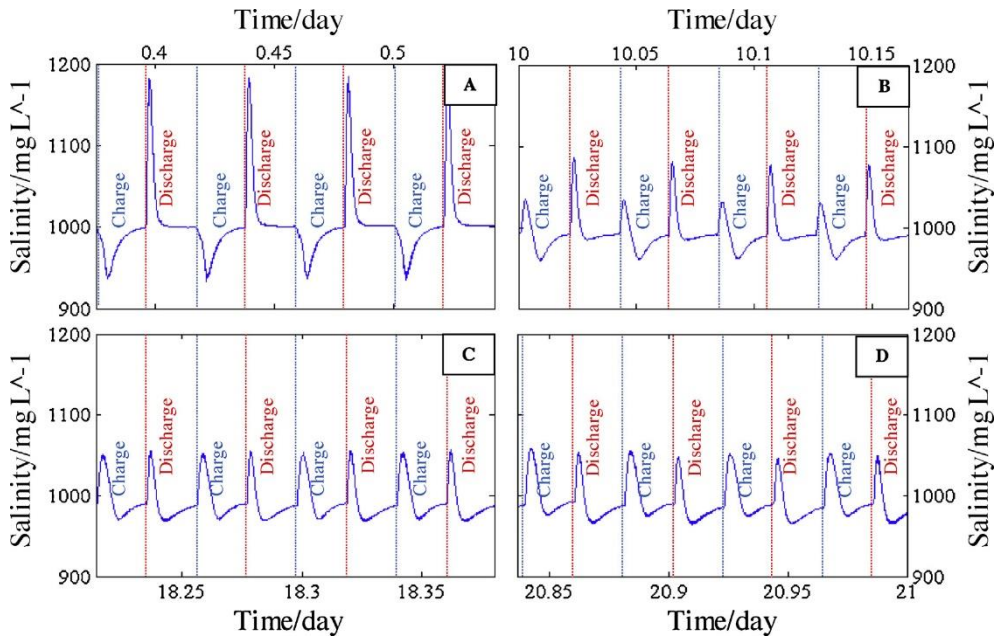

Figure 2-5 Effluent NaCl concentration in ppm vs. time in day measured during prolonged cycling. The four plots relate to selected time domains. During charge and discharge step, 0.9 V and 0 V were applied, respectively (Cohen et al., 2015).

On the other hand, it is interesting issue whether carbon oxidation is originated from oxygen (O_2) or water molecule. Cohen et al. tested long-term stability of CDI using the N_2-purged influent. As a result, the time needed for inversion peak observation and performance degradation was shortened (Figure 2-6). For example, 10 days were taken for the initial formation of inversion peak when using air-purged influent but 7 days were taken when using N_2-purged influent. Furthermore, the time needed for performance degradation, where both desalination and regeneration did not occur in charging step as well as discharging step, were lower when using N_2-purged influent than when using air-purged influent.

On the other hand, the result of long-term stability test after N2 purging showed slightly different result (Yu, 2017). As shown in Figure 2-7(a), at last 3 cycles, the fluctuation of effluent conductivity in CDI with N2-purged influent and intensity of inversion peak were larger than that in CDI. This is interpreted that the carbon oxidation occurred less after O2 removal by N2 purging because observation of inversion peak was known as an evidence of carbon oxidation (Cohen et al., 2013). Less carbon oxidation in CDI with N2-purged influent was resulted in less SAC reduction as shown in Figure 2-7(b). SAC reduction in CDI with N2-purged influent was approximately 67% while that in CDI with normal influent was 85% although it was quite lower than

that in MCDI (approximately 17%).

A reason could be found in a study by Srimuk et al. (Srimuk et al., 2016). Although the authors did not discuss in detail, they reported the improved long-term stability of CDI decorated with TiO2 which decomposes hydrogen peroxide (H_2O_2). As referred in section 2.2.2., H_2O_2 is generated at cathode by an oxygen reduction reaction (ORR). Also, it is known that H_2O_2 oxidize carbon by chemical oxidation generating oxygen functional group or causing carbo corrosion to CO or CO_2. Therefore, the result by Srimuk et al. can be interpreted that the carbon oxidation by H_2O_2 can be preserved by blocking the H_2O_2 transfer from cathode to anode.

Based on the interpretation about the result by Srimuk et al., it can be concluded that the SAC reduction of 67% (Figure 2-7(b)) was due to carbon oxidation by the reaction between carbon and water molecule and the difference of 18% (i.e. the gap between CDI and CDI with N2-purged influent) was due to carbon oxidation by the chemical oxidation of H_2O_2. That is, the most dominant source of carbon oxidation is the water molecule, but generation of H_2O_2 and carbon oxidation by H_2O_2 should be considered to improve long-term stability more.

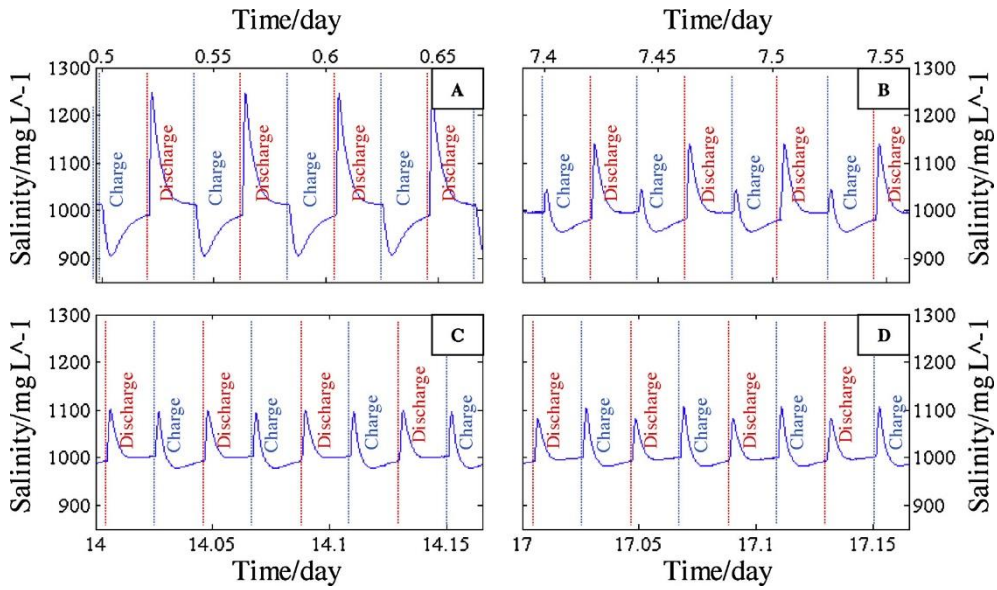

Figure 2-6 Effluent NaCl concentration in ppm vs. time in day measured during prolonged cycling using N_2-purged influent. The four plots relate to selected time domains. During charge and discharge step, 0.9 V and 0 V were applied, respectively (Cohen et al., 2015).

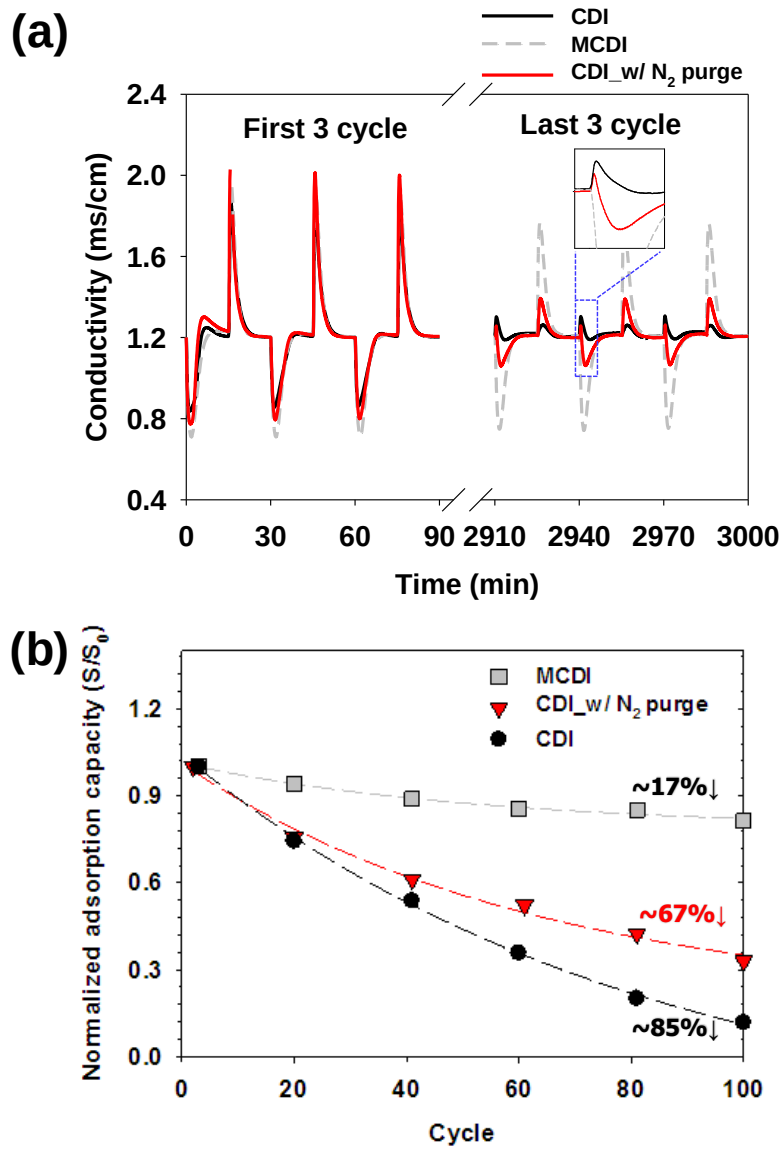

Figure 2-7 (a) Conductivity profile at first 3 cycles and last 3 cycles and (b) normalized salt adsorption capacity (SAC) of CDI, MCDI, and CDI with N_2 purging.

The mechanism for the formation of oxygen functional group have been studied and explained in fuel cell area (Avasarala et al., 2010,Bayram and Ayranci, 2011,Gurel and Ciraci, 2013,Hara et al., 2012,Hsieh et al., 2010,Park et al., 2013,Vujković et al., 2018,Yi et al., 2017). The fuel cell includes carbon substrate for oxygen reduction reaction (ORR) catalyst. It has been observed that the carbon substrate is oxidized resulting in the carbon mass loss by generating carbon monoxide (CO) or carbon dioxide (CO_2). Additionally, the oxygen functional groups such as carboxylic group, hydroxyl group, epoxy group, and so on were generated. Therefore, performance of fuel cell in terms of energy efficiency, capacity, and so on is degraded.

The direct reason of the carbon substrate oxidation has been reported that the reaction between carbon and water molecule. As depicted in Figure 2-8, various oxygen functional groups could be formed. The most important point is that water molecule let the carbon structure be more nucleophilic in acidic condition. The nucleophilic site of carbon-water complex reacts with oxygen or hydrogen inducing the formation of various functional groups.

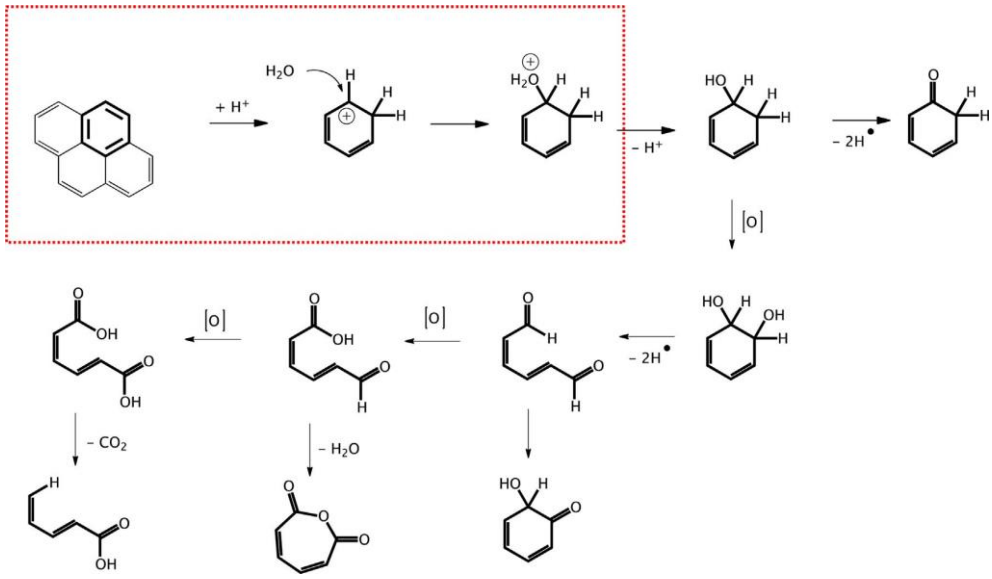

Figure 2-8 Schematic diagram for carbon oxidation and formation of oxygen functional groups (Yi et al., 2017)

The increase in carbon surface oxygen functional groups shown in Figure 2-4 results in a shift in PZC, which can be analyzed electrochemically. PZC can be measured by Cyclic Voltammetry (CV) or Electrochemical Impedance Spectroscopy (EIS), and the formation and effects of oxygen functional groups can be examined by comparing PZC of the anode before and after long-term operation.

The effect of PZC shift due to oxidation of the carbon surface on the SAC and various electrical indices can be simplified as shown in Figure 2-9. First, since PZC of both electrodes is the same at first, when 1.2 V is applied to a cell, 0.6 V is actually applied to anode and cathode, respectively. Thus, ions equivalent to 0.6 V are adsorbed. However, if the anode's PZC is slightly moved to the positive direction (Figure 2-9 (b)), the potential at each electrode moves in the positive direction because the potential window is positioned so that the amount of ions adsorbed on the anode and cathode is the same. At the same time, the actual potential applied to the electrode is substantially small, thereby reducing the number of ions adsorbed. When the PZC is moved about 0.3 V, the ions corresponding to the potential of each electrode are gradually adsorbed after the ions attached at the time of applying 0 V are desorbed. This results in a temporary increase in electrical conductivity at the beginning of potential application followed by a drop in electrical conductivity. If PZC is

moved beyond that, the number of ions attached at 0 V is greater than the number of ions adsorbed at 1.2 V. Therefore, finally, ions are adsorbed at 0 V and desorbed at 1.2 V. Inverted-CDI (i-CDI) desalting using this principle has been reported (Che et al., 2019,Gao et al., 2015,Hu et al., 2018,Oyarzun et al., 2018). As can be seen from Figure 2-9(e), if the PZC is shifted continuously by applying 1.2V in i-CDI state, the performance is expected to increase gradually, but this phenomenon has not been reported at present. .

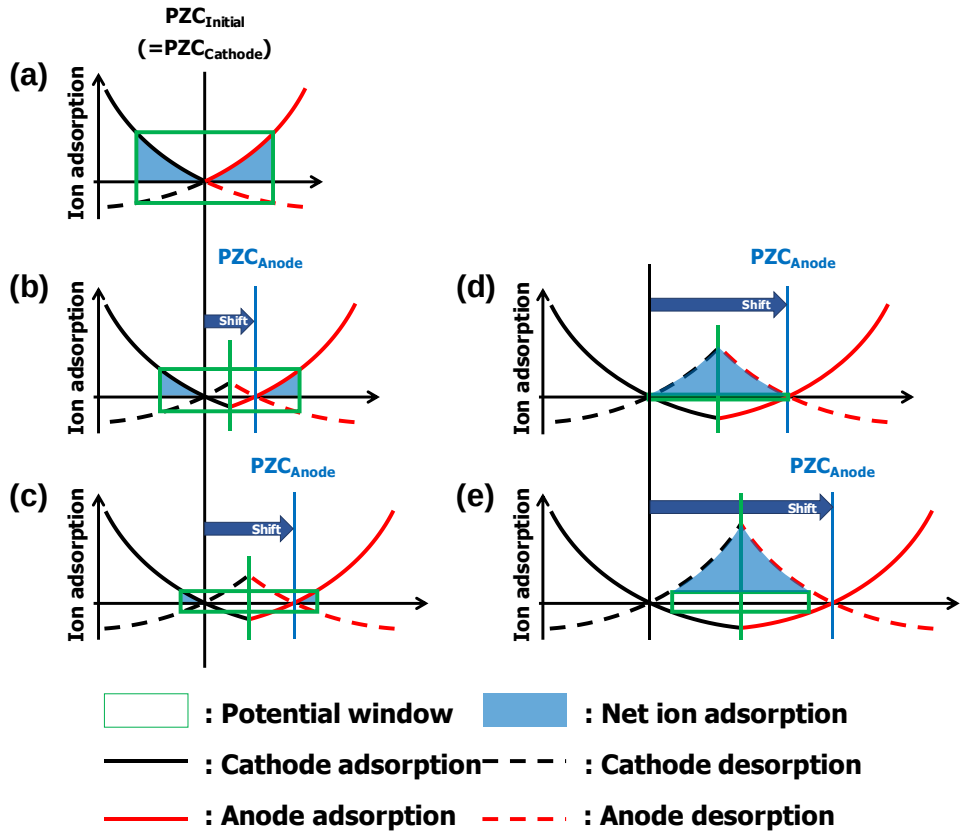

Figure 2-9 Schematic diagram for the effect of anode PZC shift. (a) Initial state, (b) first step: reduction of salt adsorption capacity (SAC) (shifted under 0.6 V), (c) second step: observation of inversion peak (shifted at 0.6 V), (d) third step: fully inversed (shifted over 1.2 V), and (e) fourth step: further SAC increase of inversed CDI (shifted over 1.2 V).

2.2.4. Attempts to improve long-term stability

There have been many attempts to improve long-term stability of CDI by adding metal oxide such as alumina and silica (Lado et al., 2015), and titania (Srimuk et al., 2016), by forming asymmetric surface charges (Che et al., 2019,Ma et al., 2019a), or by coating polyaniline (PANI) (Evans et al., 2019). Furthermore, long-term stability can be enhanced by adopting novel operating conditions (Cohen et al., 2015,Gao et al., 2017) or adding ion exchange membrane (Omosebi et al., 2017,Yu et al., 2018). Nevertheless, these reports have limitations which should be supplemented.

As studies that modified electrodes by adding metal oxide to the carbon electrode, Lado el al. (Lado et al., 2015) reported the SAC reduction of 30% after 40 h-operation. The authors insisted that calcium deposition and carbon oxidation were the main reason for the SAC reduction. However, the result of control system without metal oxides did not displayed in their system, so it is hard to trust their insist. On the other hand, Srimuk et al. (Srimuk et al., 2016) showed the improved long-term stability from 90% (conventional CDI) to 10% (TiO_2-decorated CDI) and insisted that the main mechanism for the improvement is decomposition of H_2O_2 which cause carbon oxidation. However, their insists were limitedly supported by the discussion because the important issues such as how the H_2O_2 was able to be decomposed and how

much carbon oxidation was reduced were rarely explained.

Another studies about electrode modification reported functionalization of carbon surface can improve long-term stability. For example, Che et al. (Che et al., 2019) changed surface charge of carbon electrode by forming functional groups that have positive or negative charges. Surface oxidation by acid treatment and imidazolium attachment to the surface induced the improvement of long-term stability resulting in SAC reduction of only 20% compared to that of 80% in conventional CDI. However, the surface treatment conducted by Che et al. was a kind of inverted-CDI whose working principle was reverse of conventional CDI. Therefore, this result is difficult to be applied to the conventional CDI. On the other hand, Ma et al. (Ma et al., 2019a) formed ammonium and sulfate functional group on the defect site of CNT to emulate MCDI. Although long-term stability of this system was higher than conventional CDI, there were insufficient data and discussions to investigate detailed mechanism of the stability improvement.

2.2.5. Stability of MCDI

MCDI is currently being developed as a commercial product among various CDI architectures. Therefore, evaluating and improving the long-term stability of MCDI is one of the most important issues at present. The main

difference between MCDI and conventional CDI is that an ion exchange membrane is inserted in front of the electrode. IEMs have a significant effect on ion transport between electrode and influent, resulting in different characteristics such as SAC and charge efficiency, as well as electrical properties represented by resistance. Therefore, there is a possibility that various side reactions and ion storage characteristics occurring in CDI are different. Therefore, the study of the long-term stability of MCDI is necessary separately from CDI, as reported by Omosebi et al and Yu et al.

Omosebi et al tracked changes in SAC by running CDI and MCDI for approximately 50 hours. As a result, after 50 hours of operation, CDI's SAC dropped to near zero, and an inversion peak was observed. However, MCDI showed little SAC reduction and no inversion peak (Figure 2-10(a), (b)). The reason is that the ion exchange membrane inserted into the MCDI increased ohmic resistance, preventing the MCDI's anode from oxidizing. As evidence, the increase in resistance measured by electrochemical analysis and the maintenance of charge efficiency measured in CDI operation (Figure 2-10(c)) are presented. However, this paper insisted that a small amount of anode oxidation occurred based on the measurement of charge efficiency, but did not focus on the reasons why the reaction was reduced.

Yu et al., Further from Omosebi's previous paper, attempted to

systematically investigate the principle of side reactions in CDI and MCDI by tracking changes in hydrogen peroxide and pH at the cathode. As a result of SAC comparison, as shown in Figure 2-11 (c) and (d), only 17% was decreased in MCDI, unlike CDI, which decreased SAC by more than about 90%. In addition, inversion peaks did not appear in MCDI after about 50 hours of operation. The reason is shown in Figure 2-11 (a) and (b). In the CDI, hydrogen peroxide generated at the cathode is moved to the anode to be decomposed, and the reaction generates oxygen functional groups on the surface. However, in MCDI, the path through which oxygen, a reactant of the hydrogen peroxide generation reaction, is supplied to the electrode surface is blocked, thereby generating less hydrogen peroxide and decomposition. In addition, since the ion exchange membrane acts as a significant electrical resistance compared to the carbon material and the influent water, there is an effect that the magnitude of the potential actually applied to the electrode is reduced (Choi, 2014). As a result, the reaction of carbon with water rather than hydrogen peroxide is reduced. That is, two Faraday reactions in which oxygen functional groups are generated are blocked, so that the anode is less oxidized, and thus, a decrease in SAC during long-term operation occurs.

However, there are factors that are not considered in both papers. For example, in the oxidation reaction introduced in Section 2.2.3, the reduction

potential of the reaction of carbon and water molecule to form oxygen functional group stays in the region of very low range. While the potential applied to the oxidation electrode exceeds 0.8 V versus the reference electrode, the reduction potential of the carbon oxidation reaction is only -0.4 V. Therefore, the carbon oxidation reaction can occur even if actual potential applied to the electrode is relatively low due to the ohmic resistance of ion exchange membrane. In other words, even though the reaction occurs, the effect of the ion exchange membrane offsetting the effect of carbon oxidation, so that the change in the SAC that appears as the final result looks less. Therefore, in order to confirm this, it is necessary to consider the method of protecting activated carbon without an ion exchange membrane.

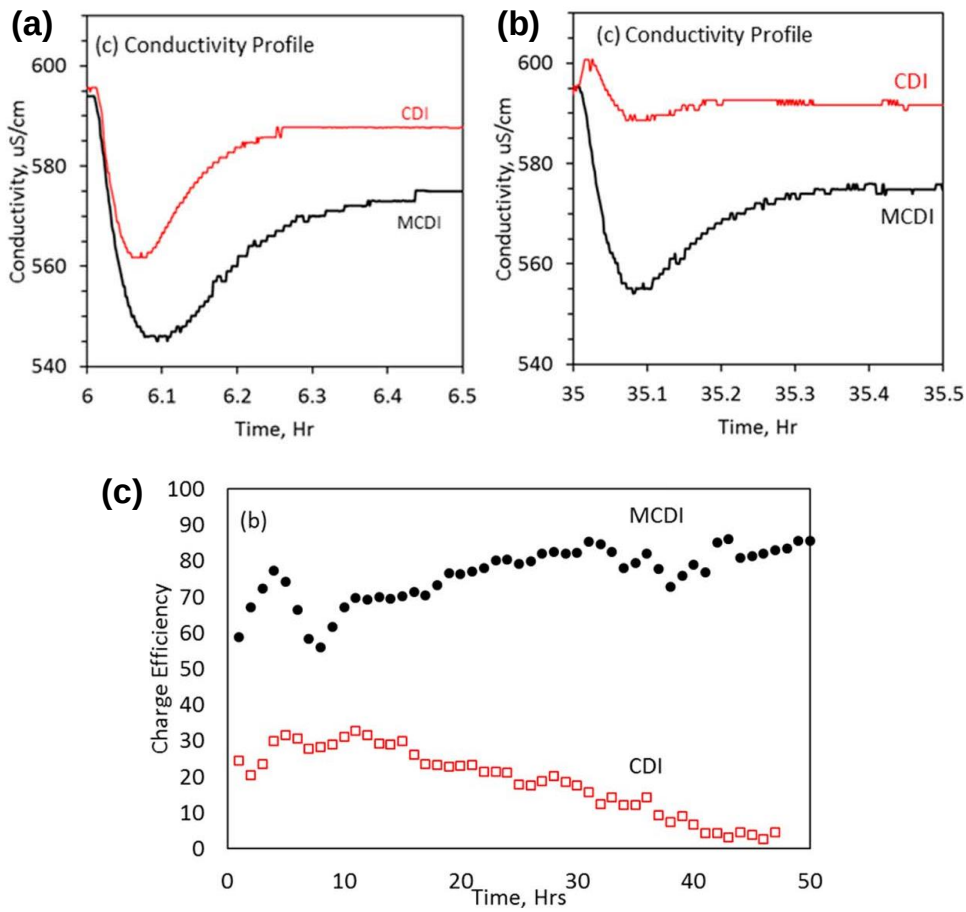

Figure 2-10 (a) Effluent conductivity profile of CDI and MCDI after 6 h operation and (b) that after 35 h operation. (c) Charge efficiency changes during 50 h operation (Omosebi et al., 2014).

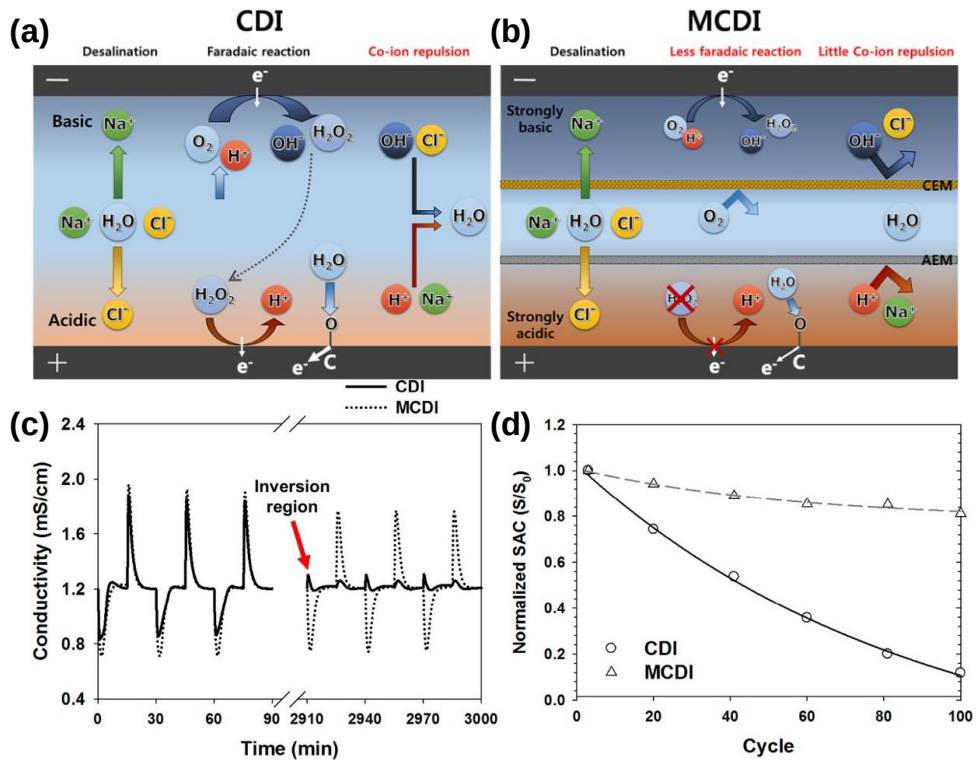

Figure 2-11 (a) Schematic diagram explaining the consumption of charges applied during charging step in CDI, and (b) in MCDI. (c) The conductivity profile of CDI and MCDI and (d) salt adsorption capacity (SAC) changes of CDI and MCDI (Yu et al., 2018).

2.3. Polymer-coated electrode for CDI

The polymers coated on CDI electrodes so far include PDA and IEP. PDA has been applied to increase the hydrophilicity of the electrode. Because the carbon material has a surface which is considerably hydrophobic, it can be expected to improve the desalination performance by increasing the hydrophilicity. IEPs have been applied to overcome two disadvantages of conventional MCDI; the expensive price and thickness of the ion exchange membrane, as a material to replace the ion exchange membrane in MCDI.

2.3.1. Polydopamine coating

PDA is a substance found in the adhesive that Mussel attaches to the stone surface and discharges to survive (Figure 2-12 (a)) (Lee et al., 2007). Dopamine molecules are a kind of neurotransmitters commonly found in humans and animals, but they are polymerized through self-synthesis (Figure 2-12 (b)) under basic conditions of pH 8.5 ~ 8.8. The most representative feature is the formation of a hard and thin polymer layer, which is mainly applied to give hydrophilicity to the surface. It has been widely applied because it is famous for coating successfully on substrates such as metals, nonmetals, polymer surfaces, etc. (Ryu et al., 2018).

The carbon surface is no exception, Xie et al. coated PDA on activated

carbon having a specific surface area of about 1700 m^2 g^{-1} and applied it as a CDI electrode. They used a variable time to coat PDA to produce a variety of PDA coated electrodes. Considering that PDA is synthesized at the material surface through self-synthesis, it is expected to thicken the PDA over time. As a result, it was observed by electrochemical analysis that the thicker coating layer was developed over time, which resulted in the reduction of the pores of the material and the increase of the electrical resistance. Therefore, thicker coatings for more than 4 hours resulted in poor desalination due to a decrease in specific surface area and an increase in resistance. However, if the coating time is shorter than 4 hours, the SAC was improved. It is because the effect of improvement in hydrophilicity overwhelmed that of pore decrease. In particular, the use of the electrode coated for 4 hours increased the SAC by about 2.6 times, showing that the effect is significant. This study confirmed the effects of PDA coating on the desalination performance of CDI in various ways, but it was considered that the study did not examine the effect on the long-term operation stability in detail.

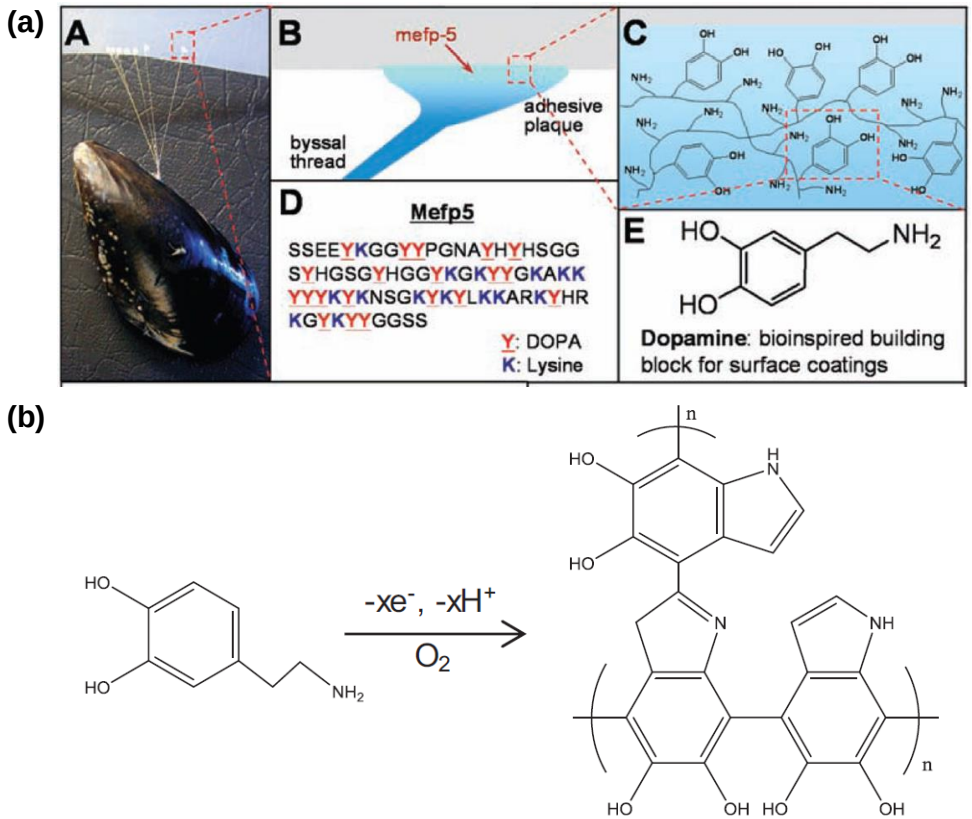

Figure 2-12 (a) Polydopamine (PDA) as a component of bioinspired adhesive plaque (Lee et al., 2007), (b) polymerization mechanism of dopamine (Xie et al., 2017)

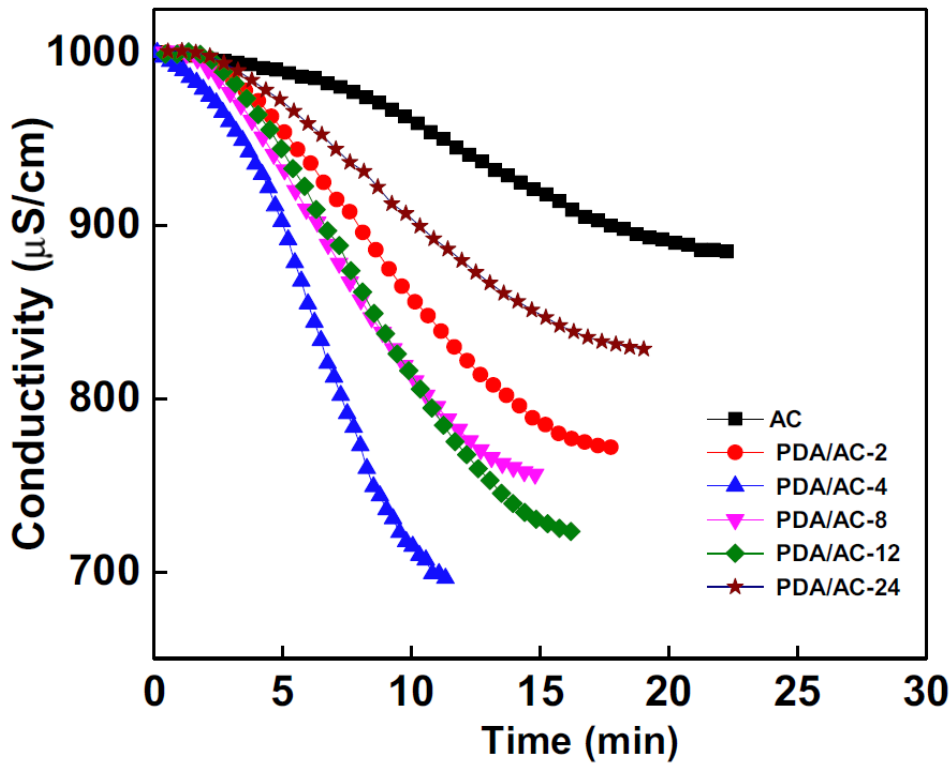

Figure 2-13 Conductivity changes of CDI using polydopamine (PDA)-coated activated carbon as an electrode material (Xie et al., 2017)

2.3.2. Polyaniline coating

Polyaniline (PANI) is a famous polymer used to form various shape of carbon and catalyst nanoparticles by templating method. Also, it is broadly used itself as a conducted polymer. Therefore, there was an attempt to apply PANI to CDI (Evans et al., 2019). The authors coated PANI to activated carbon powder and fabricated electrode. After that, they tested the long-term stability as well as desalination performance. As a result, long-term stability was outstandingly high (i.e. only 7.2% SAC reduction after 300 h). However, this result has a critical limitation that there was no control system to compare each other, which means that the effect of PANI not only be distinguished but also be believable.

2.3.3. Ion-exchange polymer coating

The application of IEPs to CDI has proceeded mainly in two ways. One is to make the synthesized polymer into a solution state and then cast or mix it on the electrode. The other is to mix monomers in a solution containing activated carbon or an electrode to be synthesized on the electrode surface in situ way. The first method was applied to most CDI electrodes using static electrodes (Asquith et al., 2014,Jain et al., 2018,Kim and Choi, 2010a,Kim and Choi, 2010c,Li et al., 2017) and second method was applied to FCDI that activated

carbon powders should be dispersed in the water particle by particle (Park et al., 2016).

Most of the literatures about IEPs coating on activated carbon electrode have focused on improving SAC and improving charge efficiency, as shown in Figure 2-14. This is because the purpose of the IEP coating is to replace the ion exchange membrane. In literature, this goal has been successfully achieved and despite the slightly higher resistance, SAC has been greatly improved (Kim and Choi, 2010c). The IEPs used in these studies are generally materials in which commercial IEPs are dissolved in a solvent, and in some studies, two monomers were mixed directly in various ratios to increase the hydrophilicity of the IEPs (Asquith et al., 2014,2015).

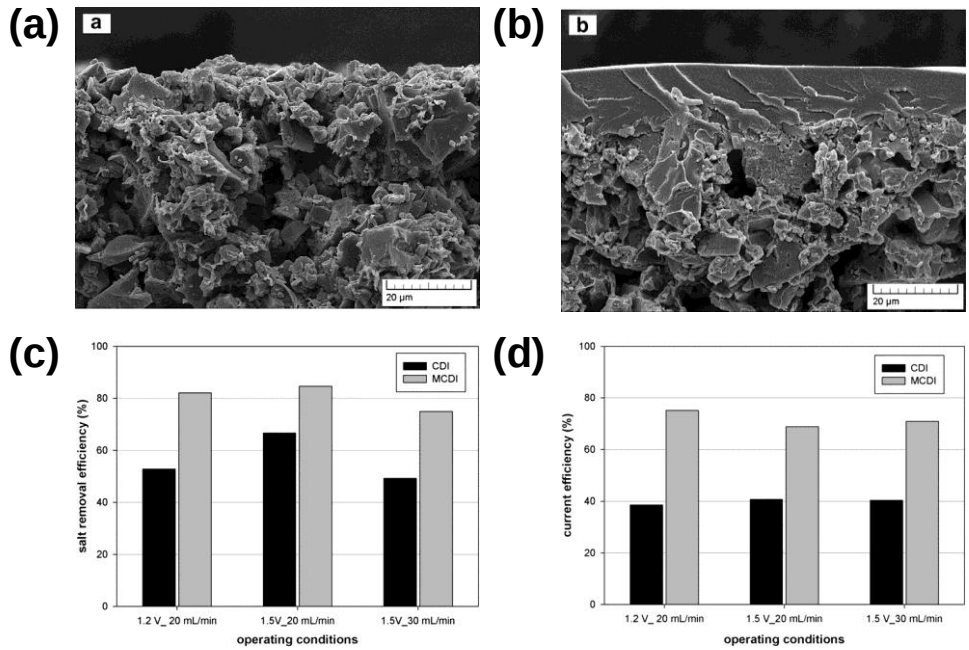

Figure 2-14 (a) Cross section SEM image of pristine AC electrode and (b) that of ion-exchange polymer (IEP)-coated electrode. Comparison result of (c) salt removal efficiency (equal to SAC in this thesis) and (d) current efficiency (equal to charge efficiency in this thesis) (Kim and Choi, 2010c).

Unlike conventional CDI, the advantage of MCDI or IEP-coated CDI is that CDI can be given selectivity for specific ions depending on the feature of IEP for coating. This method is mainly used to composite anion-selective CDI, since the cation-selective CDI can be achieved by utilizing the battery material as the electrode material. In case of nitrate-selective CDI, commercial nitrate selective IEP was mixed with PVDF binder followed by coating on the electrodes. (Kim and Choi, 2012).

As reviewed, researches on PDA and IEP coatings have been continuously conducted and the polymer coating has achieved improvements in SAC and charge efficiency. However, the effect of the polymer coating on the long-term operation stability of the CDI is insufficient.

2.4. Limitations of previous studies

Through the chapter 2 from section 2.1 to section 2.3, lots of studies related to long-term stability of CDI were introduced. However, there were two critical limitations that should be overcome.

First, few papers focusing on improving long-term stability have been published (i.e. four papers; (Cohen et al., 2015,Evans et al., 2019,Gao et al., 2017,Srimuk et al., 2016)). Furthermore, those papers focused on not preventing carbon oxidation but utilizing the result of carbon oxidation such as surface

charge change and H_2O_2 generation. This means that the potential possibility of further SAC reduction is still involved because carbon oxidation reactions still occur, though improvement in long-term stability was observed in some cases. In consideration that the most fundamental problem is the carbon oxidation reactions between carbon and water molecule, the most accurate and effective solution is to prevent the reactions from occurring. Although there could be various solutions, the best way is to block carbon and water molecule meet each other or to form conditions so that the reactions do not occur. The latter solution was introduced as the concept, 'maximum allowable charge (MAC)' (Choi and Yoon, 2019,Yoon and Choi, 2018), that indicates the maximum charges before the Faradaic reactions occurring. When applying charges lower than MAC, the occurrence of Faradaic reactions, represented by carbon oxidation reaction, can be prevented resulting in improvement of long-term stability. On the other hand, there have been few papers focusing on the former solution.

Second, the studies about the effect of polymer coating on long-term stability was insufficient. As mentioned above, blocking carbon and water molecule from meeting each other is an effective way to improve long-term stability by solving a fundamental problem. Polymer coating on CDI electrodes, which is the main idea of this dissertation, can be one of the best

ways to block the reactants (i.e. carbon and water molecule) from meeting. However, the literatures about polymer coating have focused on the properties and effect of polymer on SAC or charge efficiency rather than the long-term stability (Asquith et al., 2015,Jain et al., 2018,Kim and Choi, 2010c,Lee et al., 2011,Nugrahenny et al., 2013,Xie et al., 2017). For example, Asquith et al. {Asquith, 2015 #1410} synthesized and coated novel IEP on the carbon electrodes. Nevertheless, they only reported the electrical properties measured by electrochemical analyses such as CV and EIS. As another example, Jain et al. {Jain, 2018 #588} coated polyvinyl alcohol (PVA)-based IEP with aqueous solvent. Because the novelty of that paper was on 'aqueous' process, they focused on the IEP's coating properties and the performances such as SAC and charge efficiency. That is, it is acceptable that polymer coating on CDI electrode was effective method to improve desalination performance of CDI, although the effect of polymer coating on long-term stability have not been investigated.

Therefore, it is necessary and meaningful to evaluate long-term stability of CDI using polymer-coated electrode and to investigate the effect and reasons of polymer coating.

3. Long term stability of CDI with polymer-coated electrode

3.1. Backgrounds

Figure 3-1 is a graphical representation of what happens when the carbon electrode surface is coated. As discussed in the literature, the SAC of CDI decreases over time because the carbon on the surface of the anode reacts with water molecules to oxidize (on the right side of Figure 3-1 and Rxn (3) ~ (6)). Therefore, by coating the surface of the anode with a material other than carbon, it is possible to prevent the oxidation of carbon and thereby improve long term stability (on the left side of Figure 3-1). Various polymers can be applied to coat the activated carbon. Considering that CDI is an electrical system, it should be concerned that the polymer's resistance may degrade the electrical properties of the electrode. Therefore, when using a nonconducting polymer, a material that can be coated as thin as possible should be selected. A material that does not degrade desalination performance by having sufficient ion conductivity even with high electrical resistance is also suitable as an electrode coating material of CDI.

The materials chosen against this background are PDA and IEPs. As described in Section 2.3.1, PDA is a thin, evenly coatable material, and the IEP is ion-conductive, so it is not expected to significantly compromise the electrical properties of CDI. According to the paper reviewed in Section 2.3.2,

the role of IEM or IEP layer is also considered to be significant considering the significant improvement in long term stability even in MCDI using IEM without activated carbon coating.

Accordingly, the purpose of this chapter is to investigate the influence of carbon oxidation at the anode by inhibiting the exposure of surface carbon to water molecule and by excluding a certain effect of ion exchange membrane. For that purpose, the long-term stability of the activated carbon electrode coated with PDA or IEP without forming IEP layer.

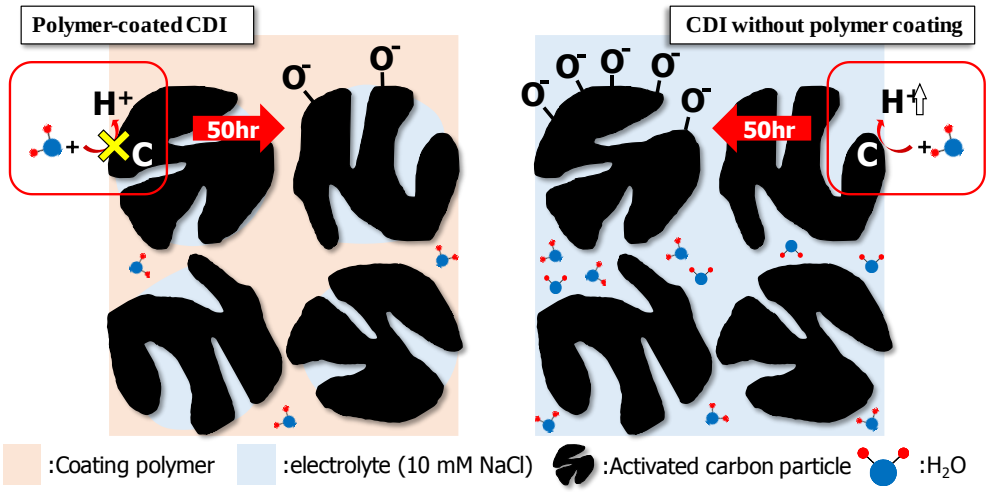

Figure 3-1 Schematic diagram of the effect of polymer coating on carbon electrode.

3.2. Materials and method

3.2.1. Electrode fabrication

Carbon electrode was consisted of the activated carbon (MSP-20X, Kansai Coke and Chemicals, Japan), super P as a conductive material (Timcal co., Switzerland), and PTFE as a binder (Sigma-Aldrich, USA) with 86:7:7 of weight ratio. Three materials were mixed and kneaded together followed by roll-pressing (MP200, Rotech, Republic of Korea) to a thickness of 300 μm. The specific surface area and total pore volume of activated carbon were about 2266 m^2 g^{-1} and about 0.79 cm^3 g^{-1} measured with N_2 adsorption /desorption method (ASAP2010, Micromeritics, USA), respectively.

3.2.2. Polymer coating

The electrodes were modified with PDA to increase the surface hydrophilicity [27-29]. For crafting the PDA solution, 2 g L-1 of dopamine hydrochloride (Sigma-Aldrich, USA) was dissolved into 15 mM Tris buffer solution at pH 8.8 (Sigma-Aldrich, USA). As dopamine is self-polymerized in an alkaline condition, the dopamine solution was immediately poured onto an electrode in a petri dish. The dopamine solution containing the electrode was gently mixed on a rocker platform (RK-1D, Daihan Scientific, Republic of Korea) for 1 h. The PDA-modified electrodes were washed thoroughly

with DI water to remove any residual PDA solution.

For IEP coating, two types of IEP were used; INC-ICS for cation-exchange polymer and INC-ITA for anion-exchange polymer (Innochemtech, Republic of Korea). Note that INC-ICS and INC-ITA are sulfonated and aminated polypropylene oxide (PPO), respectively. Approximately 2 mL of IEP was poured onto the carbon electrode put on the glass plate and silicon mold having a rectangular shape with 70 mm length, 40 mm width, and 2 mm height. After pouring, carbon electrode with IEP was put at room temperature for 12 h and dried under 70°C during 12 h. The dried electrode was stored in DI water. For the experiment, the electrodes were soaked in the influent over 12 h.

3.2.3. Electrode characterization

The surface and cross section morphologies of carbon electrode and IEP-coated electrode were analyzed using field-emission scanning electron microscope (FE-SEM, SUPRA 55VP, Carl Zeiss, Germany). The physical properties of the two ACs, including the total specific surface area (SSA) and the pore volume, were measured by N_2 adsorption isotherms (ASAP 2020, Micromeritics, USA) at -196 °C temperature after degassing them at 110 °C for 2 h and the isotherm data were calculated with the Brunauer–Emmett–

Teller (BET) equation. As electrochemical analyses, the cyclic voltammetry (CV) analysis was carried out using a three-electrode cell. The cell was consisted of a pristine carbon electrode or IEP-coated carbon electrode as a working electrode, a carbon electrode having about four times heavier mass as a counter electrode, and a reference electrode (Ag/AgCl (KCl sat'd)). The CV was conducted to measure the PZC in a range of – 0.4 ~ 0.6 V (vs. Ag/AgCl (KCl sat'd)) with 2 mV s^{-1} of scan rate using a potentiostat (VersaSTAT 3, Princeton Applied Research, USA) for three cycles. The third cycle was used to find the PZC from the average value of the potential at the minimum current flowed during oxidation step and the maximum current flowed during reduction step [20].

3.2.4. Desalination test

The CDI cell was prepared with the circular carbon electrode (20 mm in diameter and 300 μm in thickness) and inserting a nylon spacer having a diameter of 25 mm and a thickness of 200 μm between a pair of electrodes. For operating the PDA-CDI and PC–CDI, the polymer-coated electrode were assembled instead of pristine carbon electrode. The influent was 10 mM NaCl solution and the flow rate was set at 2 mL min^{-1}. The electrical conductivity

(3574-10C, HORIBA, Japan) and pH (9618-10D, HORIBA, Japan) of effluent were measured in real time and the analyzed effluent was thrown away. Note that pH was measured to modify the effluent conductivity affected by H^+ and OH^-. Voltage was applied using a battery cycler (WBCS3000, WonATech, Republic of Korea) for 10 min each at 1.2 V in the charging step and 0 V in the discharging step. A charging/discharging cycle was repeated 150 times (totally 50 h). For monitoring the potential applied to the anode and cathode separately, the reference electrode (Ag/AgCl (KCl sat'd) was inserted into the cell, and connected to an additional battery cycler.

As a representative performance of CDI, the SAC (SAC) was evaluated by Eq (1) for all cycles (totally 150 cycles)(Yu et al., 2018):

$$SAC\ \ (mg\ \ g^{-1}) = \frac{Q \cdot M_w \cdot \int (C_{in} - C_{out})dt}{m} \qquad \text{Equation (1)}$$

where C_{in} and C_{out} are the influent and effluent concentrations of NaCl (mM); Q is the flow rate (L min^{-1}); M_W is the molecular weight of NaCl (58.443 g mol^{-1}), and m is the electrode weight (g). In this study, the mass of carbon electrode except the mass of IEP was applied to the SAC calculation in both CDI and IEP–CCDI because the base carbon electrodes for CDI and IEP–CCDI were fabricated in the same carbon dough.

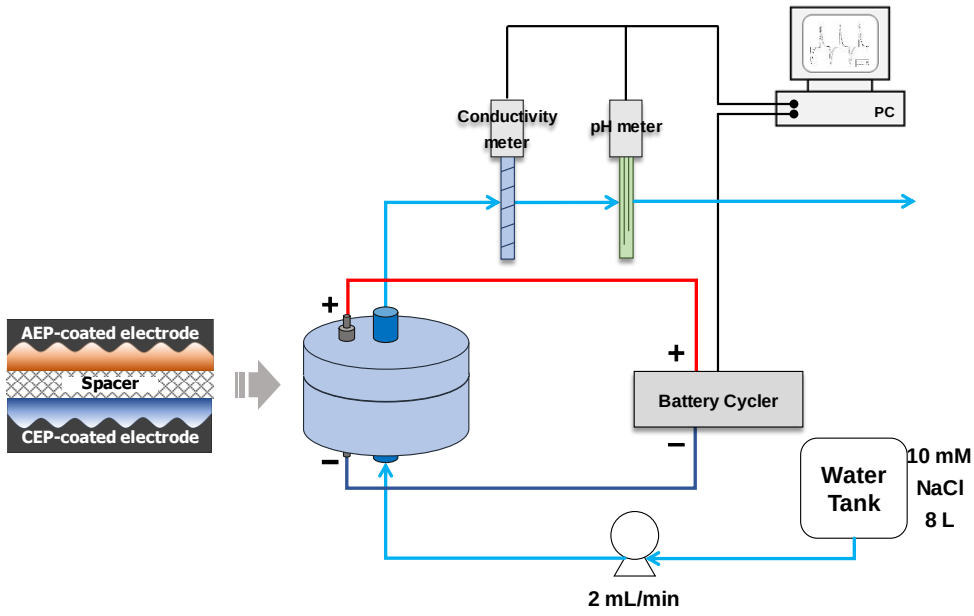

Figure 3-2 Schematic diagram for desalination test setup.

3.2.5. Anode replacing long-term operation

After CDI operation without any polymer coating for 3, 6, 9, 12, 15 and 21 hours, the anode was replaced with a pristine electrode but the cathode was not changed. Anode replacement was performed by temporarily stopping the experiment, replacing the anode with new pristine electrode, reassembling the cell, and starting operation again. Note that each step after anode replacement were named as replacing stage. All operating conditions other than cell assembly were used in the same way as described in Section 3.2.4. After all operations, the anodes oxidized for 3, 6, 9, 12, 15, and 21 hours and the cathode operated for a total of 66 hours were obtained, and PZC was calculated by electrochemical analysis of these six anode samples.

3.3. Results and discussion

3.3.1. Anode replacing long-term operation

At first, anode replacing experiment was conducted in order to confirm the influence of the oxidation of the electrode on the SAC reduction of CDI in the experimental environment of the present study, and to examine the relationship between the change of PZC, SAC value, and SAC reduction. Figure 3-3 shows the effluent electrical conductivity changes during whole anode replacing long term operation. As can be seen in the figure, after replacing the anode after the specified time, the SAC recovered to the same

level as the first time followed by gradual reduction in the amplitude of electrical conductivity, which is consistent with the general CDI behavior mentioned in the literature review. These results indicate that the cathode of CDI has very little effect on the reduction of SAC during long-term operation.

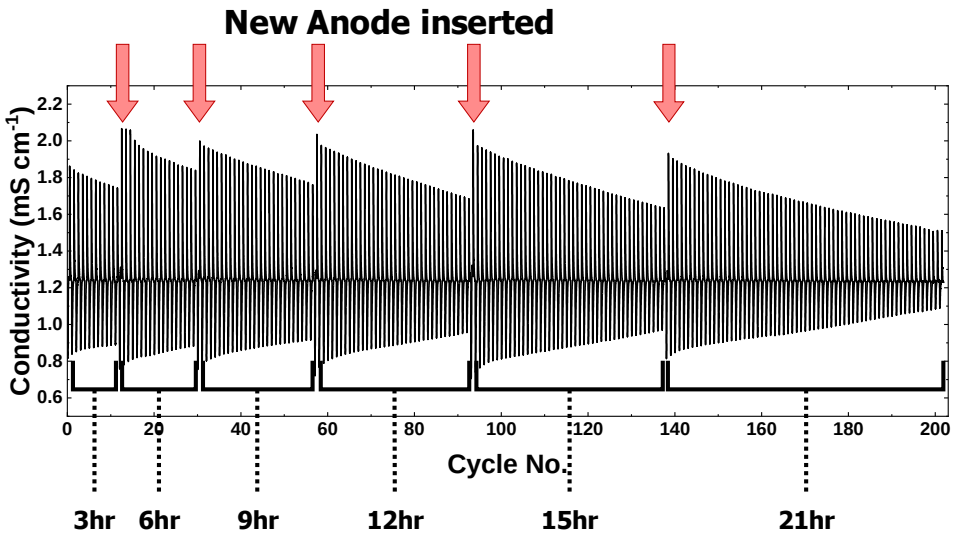

Figure 3-3 Conductivity change in anode-changing long term operation

Figure 3-4 shows the results of measuring the PZC of the electrodes obtained by CV at each replacing stage to correlate the recovery and reduction of the desalination performance. As can be seen in Figure 3-4 (a), the overall shape follows the CV behavior of the representative CDI electrode, which is commonly observed as a near rectangular shape. In detail, there was an absolute current decrease followed by increase showing a minimum current value (Figure 3-4(b)), especially, in the electrode operated for 3 hours and 6 hours. PZC is obtained by reading and averaging the voltage at which the absolute value of the oxidation and reduction current is minimum. However, the minimum absolute value of reduction current was not observed in the CV profile of the anodes operated for 9, 12, 15, and 21 hours. Instead, the current only increases as the potential move on to the negative direction, and the slope becomes steep as the driving time increases. This behavior is considered to be another phenomenon of electrode oxidation, but the interpretation of this is considered out of scope in this study. However, instead of linearly increasing the current, there is an inflection point where the slope suddenly becomes steep. PZC is obtained by reading the potential corresponding to this inflection point and calculating the minimum current potential value and the intermediate value measured in the oxidation section. When this method is used, it is considered to be a reliable method because in all cases measured

by the researcher, the minimum current potential value and the value within the range of ± 10% were measured in the oxidation section.

The PZC value read from the CV data is shown according to the time taken for operation (Figure 3-4 (c)). As shown in this figure, the PZC increased almost linearly as the operation time increased. As a result of the linear trend line, the R^2 value was about 0.92, which proved sufficient relationship. Next, to understand the relationship between PZC and SAC, SAC and SAC reduction ratios are shown for PZC (Figure 3-4 (d)). In this figure, as PZC increases, SAC decreases gradually, and the SAC reduction rate tends to increase, and the relationship also appeared to be linear.

PZC values and relationship between PZC and SAC obtained from CV can be interpreted as follows. First, since PZC increases linearly with operation time and SAC decreases linearly with PZC, it can be concluded that SAC will decrease almost linearly with time. Considering that the PZC shift and SAC reduction of occurs due to electrode oxidation, it is believed that the electrode oxidation reaction causing the PZC shift occurs constantly and continuously while 1.2V is applied. Because of this, we can expect SAC to eventually reach zero. Therefore, there is a need for a means of preventing SAC reduction by preventing such electrode oxidation, and as summarized through the literature review, the present invention has partially achieved the

purpose of preventing electrode oxidation by adding an ion exchange membrane.

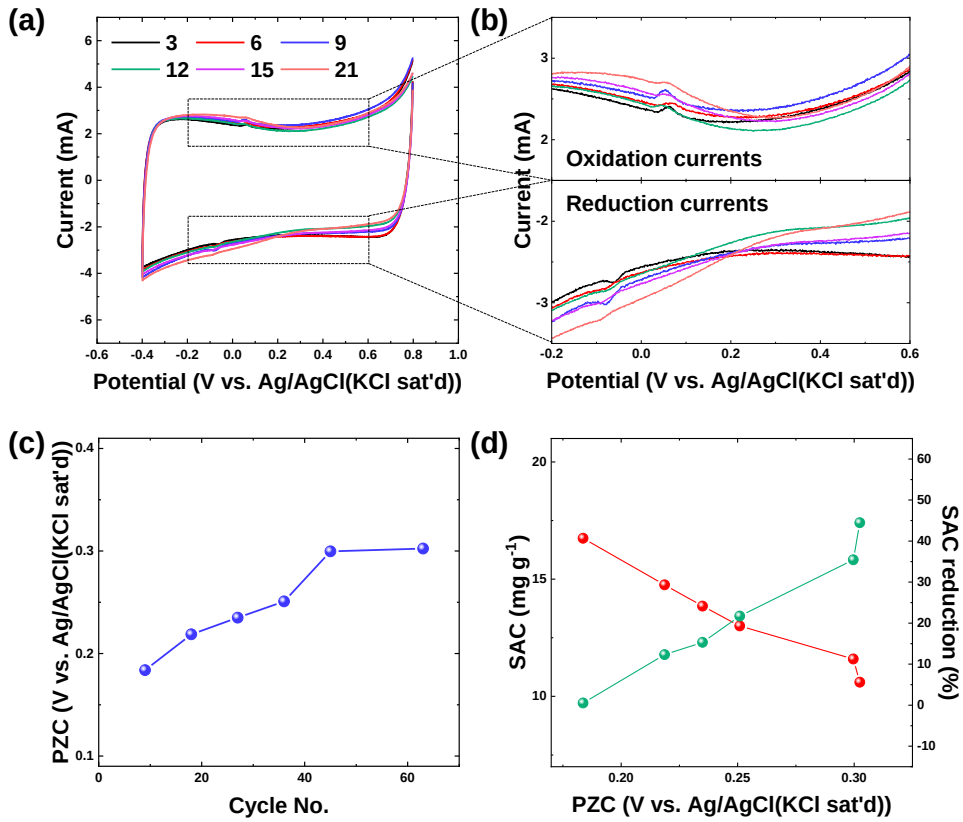

Figure 3-4 (a) Cyclic voltammetry (CV) profile, (b) enlarged oxidation current and reduction current showing potential of zero charge (PZC), (c) PZC changes by repeated cycles, and (d) changes of salt adsorption capacity (SAC) and SAC reduction versus PZC

3.3.2. Polydopamine coating

PDA was coated on activated carbon to see if electrode oxidation could be prevented by coating the surface of the activated carbon. At first, contact angle analysis was performed to check whether the PDA is coated because the most differentiated characteristic of PDA is good hydrophilicity. As shown in Figure 3-1, the contact angle was 125° before the PDA coating, but the contact angle was 78° after the coating. Therefore, it is judged that PDA was successfully coated on the electrode.

SEM images of the PDA-coated electrode showed no significant difference (Figure 3-6). Since PDA is known to be coated with a thickness of 25-50 nanometers in synthesis in the experimental conditions used in this study (Ryu et al., 2018), it can be understood that it is not noticeable on SEM. Also, when comparing Figure 3-6(a) and (b), no polymer layer was found at the electrode's outer surface (i.e. not activated carbon surface). It is because PDA is synthesized on the carbon surface by self-polymerization and the thickness of PDA coating layer is known as being limited. Therefore, the thick PDA layer could not be grown like IEP. In case of IEP, a thick layer is formed on the electrode because a highly viscous solution is used to coat the IEPs (Kim and Choi, 2010a). For the purpose of this chapter, the phenomenon that PDA does not form an additional layer is suitable for the study.

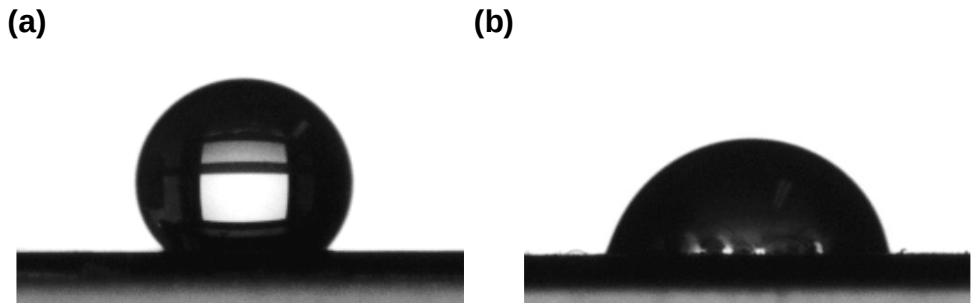

Figure 3-5 Contact angle image (a) before and (b) after PDA modification

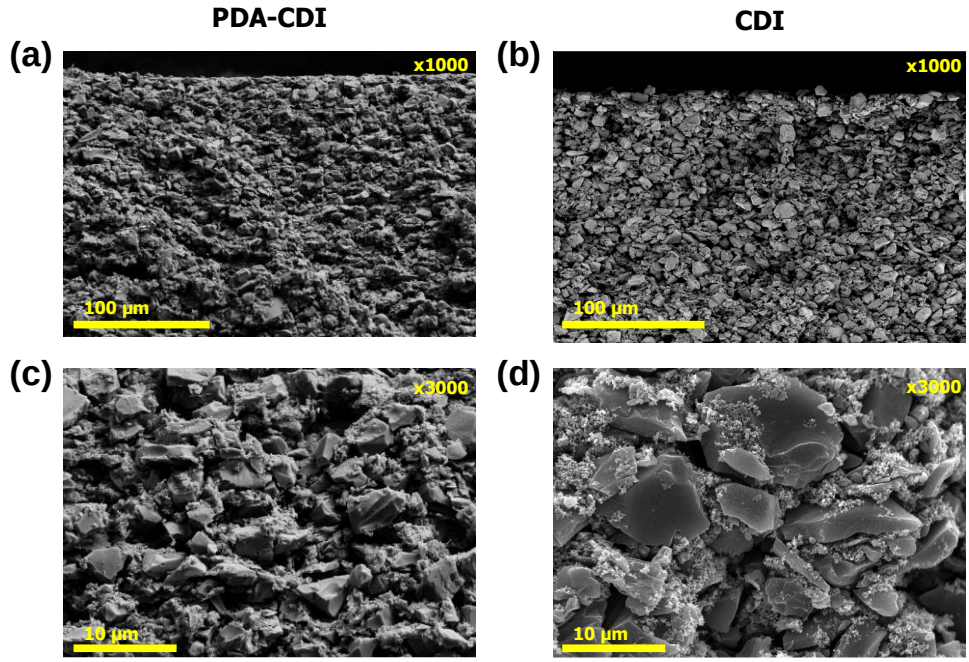

Figure 3-6 Cross section SEM images of polydopamine (PDA)–coated electrode with (a) 1000 and (c) 3000 magnifications and that of pristine electrode with (b)1000 and (d) 3000 magnifications

The long-term operation using the PDA-coated electrode is shown in Figure 3-7. Figure 3-7 shows the change in electrical conductivity over time for PDA–CDI (Figure 3-7 (a)) and CDI (Figure 3-7 (b)). As can be seen from the figure, it can be seen that both systems have significantly reduced amplitude in electrical conductivity. However, in PDA-CDI, the decrease was less, and in later cycles, the conductivity was larger than that of CDI. In particular, the difference is prominent in Figure 3-7(c) and (d), which are enlarged figure of the final three cycles. In PDA-CDI, there was a decrease in performance but no inversion peak was observed, whereas in CDI, inversion peak was observed as reported in the literature.

Figure 3-8 shows the change in SAC calculated from the change in electrical conductivity as the cycle progresses. Both systems showed similar initial SAC, but after about 30 cycles, the decrease in SAC of PDA–CDI was retarded, resulting in a SAC reduction of about 88%. On the other hand, SAC of CDI was reduced by about 99%, reaching a level where almost no ions were adsorbed. In other words, the SAC of PDA–CDI decreased less compared to CDI, and this result is evidence that PDA can prevent the oxidation of electrode occurring. In addition, it can be said that the coating of activated carbon with a polymer other than PDA shows the possibility of preventing carbon oxidation and further improving long-term stability.

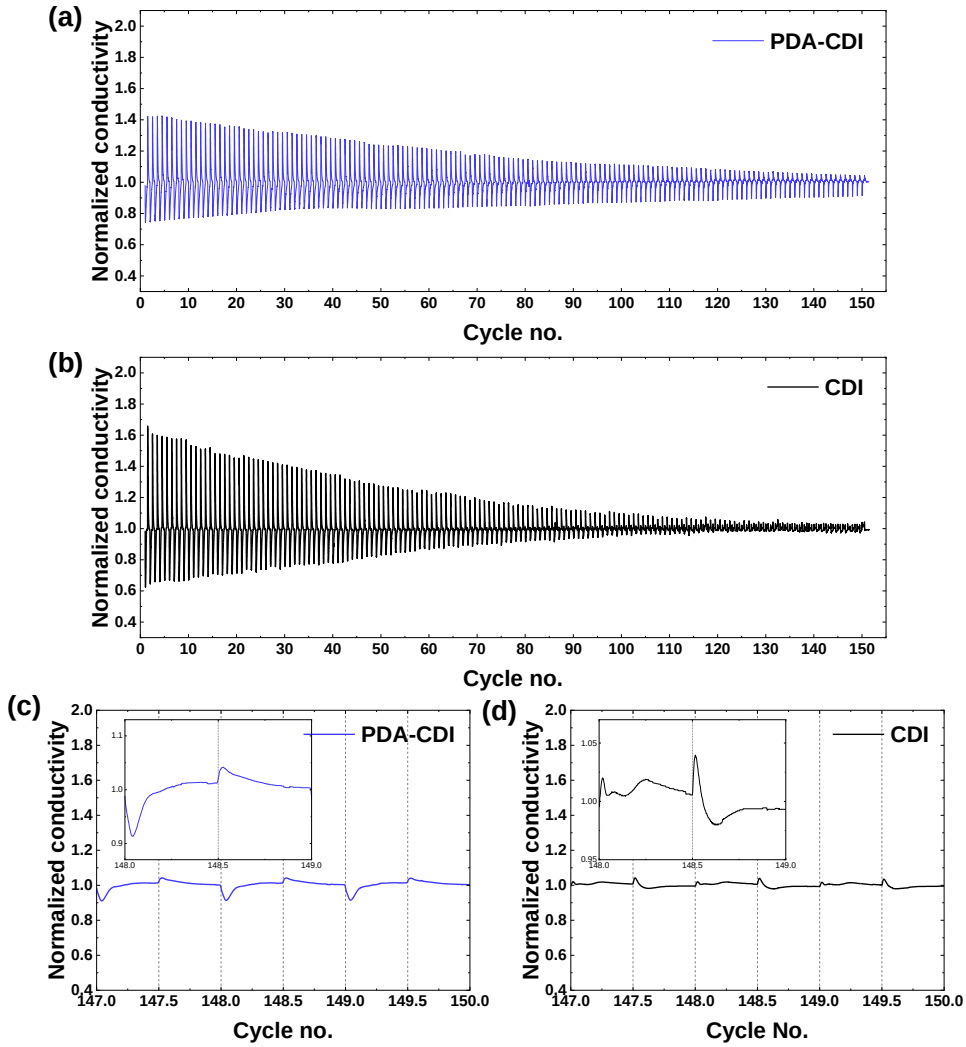

Figure 3-7 Normalized conductivity during long-term operation of (a) PDA-CDI and (b) CDI without coating

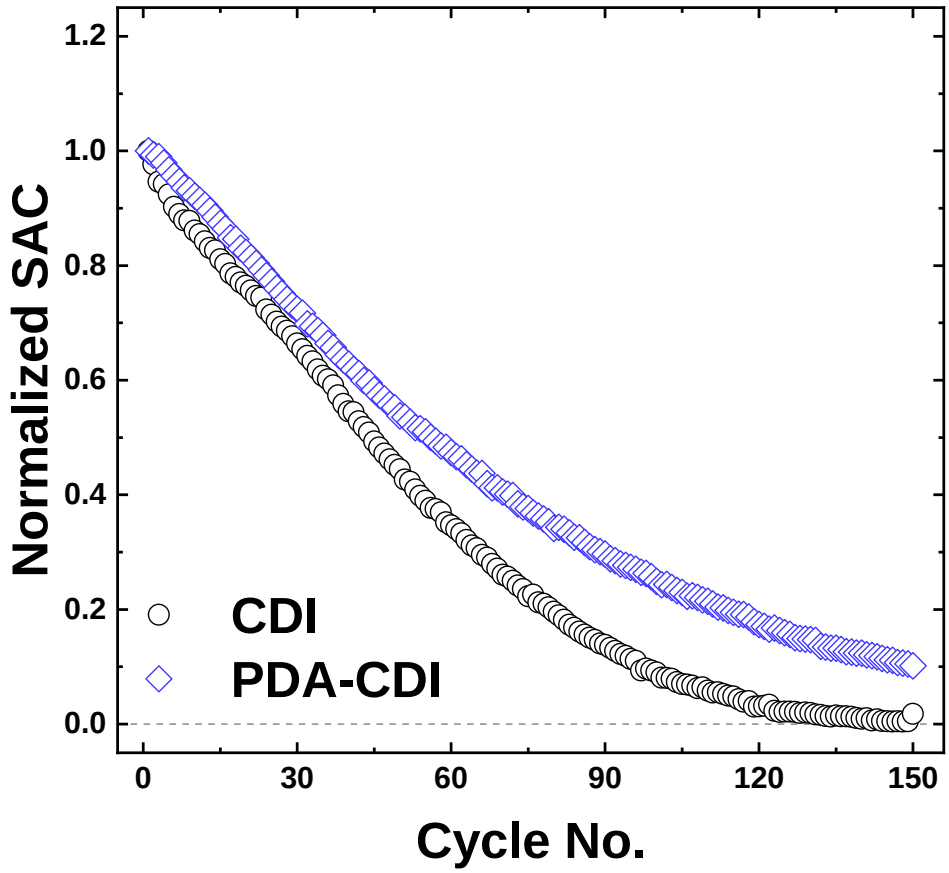

Figure 3-8 Comparison of normalized salt adsorption capacity (SAC) changes before and after polydopamine (PDA) modification

PZC measurements were performed via CV to determine how much electrode oxidation was prevented by PDA coating. There are three main types of information that can be read from CV: PZC, capacitance, and relative electrical resistance. PZC can be compared by reading the potential which shows the lowest electric current value in an oxidation range and a reduction range, respectively. The capacitance can be calculated and compared with each other by comparing the magnitude of the current among the CV profiles measured at the same scan rate. Finally, the magnitude of the relative electrical resistance can be compared with the rate of slope of current change at the point of transition from oxidation to reduction or reduction to oxidation.

First, PZC measurements showed that the PDA–CDI electrode (Figure 3-9 (a)) showed a PZC of 0.20 V before long-term operation, but PZC of PDA–CDI was shifted by 0.14 V to 0.34 V after long-term operation. On the other hand, that of CDI was shifted by 0.3V from 0.07V to 0.37V. Thus, PDA coatings can be said to reduce the oxidation of the electrode by half. In addition, PZC of PDA–CDI electrode has higher value in positive direction than CDI electrode before long-term operation. It is because the carbon surface is more negative than the surface charge of the original activated carbon (see Figure 2-9) since the PDA is itself negatively charged. Second, it is possible that the PDA acts as an electrical resistor because it is an insulator.

This can be confirmed in part by the rate of change of current when the direction of potential progression changes in the CV result. In an ideal capacitor, the CV result will be a perfectly rectangular shape. However, in a real cell, there is electrical resistance which limits the current flow. In consideration that the electrolyte used in the CV experiments in this study was a 1 M NaCl aqueous solution, which means that the ions are present in a sufficiently high concentration, the diffusion of ions is not a rate determining component. Therefore, due to the electrical resistance of the cell, it is possible that the all oxidation currents are all shifted in the positive direction and the reduction currents are all shifted in the negative direction. In other words, the rectangular shape of CV result was changed to parallelogram shape.

Next, as a result of the comparison of capacitance, the capacitance of PDA–CDI was measured larger. About 137 F g^{-1} was measured for CDI, while about 151 F g^{-1} for PDA-CDI. This is due to the increased hydrophilicity of the electrode. The PDA coating utilized the specific surface areas in the micropores which was not fully utilized (Aslan et al., 2016,Kim et al., 2014,Xie et al., 2017). After long-term operation of both electrodes, the capacitance values of both electrodes were found to decrease in common. The capacitance values of PDA–CDI and CDI were 141 F g^{-1} and 132 F g^{-1}, respectively. Both values are about 7% and 3% lower than before long-term operation. This result can

be interpreted that carbon oxidation and PZC shift occurred as a result of long-term operation is not absolutely related to the degradation of the SAC in the CDI experiment. In other words, the changes in electrochemical properties of the electrode itself were not significantly affect to the degradation of the SAC. These results can confirm again that the SAC reduction of CDI is due to an imbalance that occurs while only the PZC of the anode is shifted while the PZC of the reduction electrode is maintained.

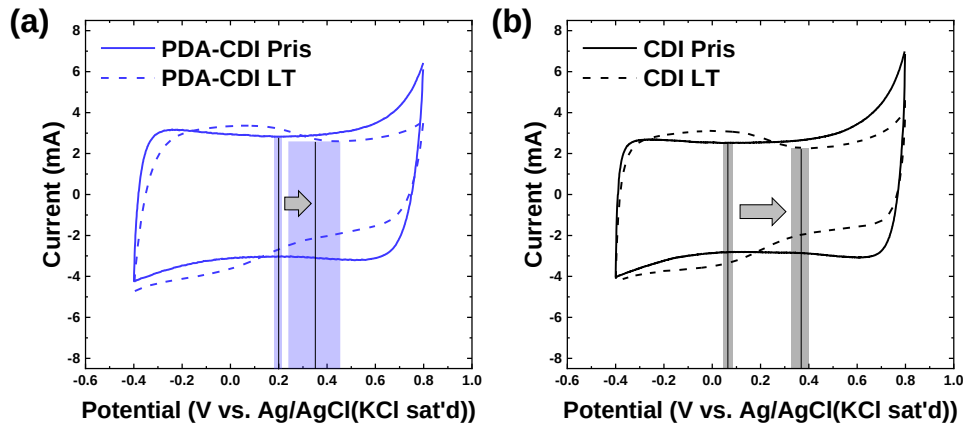

Figure 3-9 Cyclic voltammetry result of (a) PDA-CDI and (b) CDI before and after long-term operation

3.3.3. Ion-exchange polymer coating

Figure 3-10 (a) shows the normalized SAC of PC-CDI for long-term operation. Compared to the CDI or PDA-CDI shown in Figure 3-7, the change in the amplitude of effluent conductivity was very small. In addition, the early and late electrical conductivity profiles shown in Figure 3-10(c) and (d) was hardly different. This small change can be quantitatively determined by the change in the SAC cycle (Figure 3-10(b)). In the case of PC–CDI (red squares), the SAC of 16.8 mg g^{-1} was initially measured, but as the cycle repeated, SAC decreased steadily and was finally dropped to approximately 20% (13.2 mg g^{-1}). This was 80% higher value compared to the changes in the SAC of CDI (black circle) and PDA–CDI (Figure 3-7).

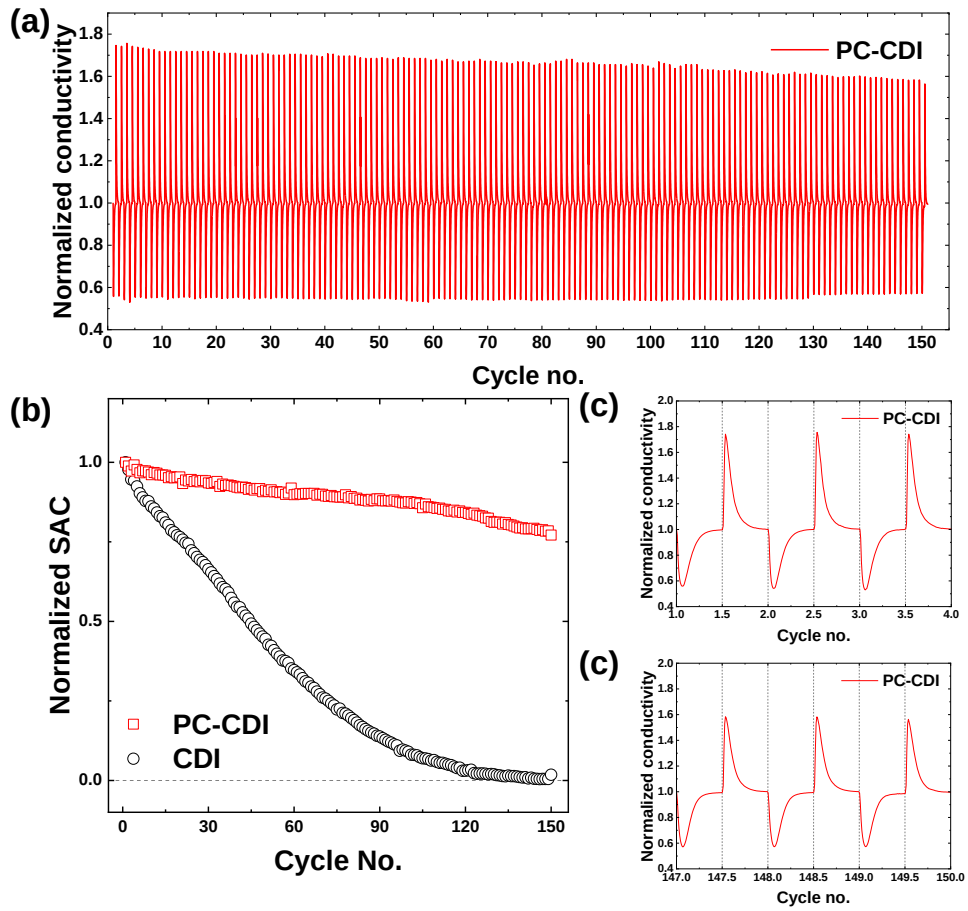

Figure 3-10 (a) Changes in conductivity profiles and (b) salt adsorption capacity (SAC) of CDI and PC–CDI during 150 cycles of operation. (c) Enlarged conductivity profile at early cycles and (d) that at later cycles.

In order to investigate the PZC shift of PC–CDI electrode, CV was carried out. (Figure 3-11(a)). As a result, the PZC of PC–CDI shifted by 0.06 V from 0.26 V to 0.32 V indicating that there were little carbon oxidation reactions at the PC–CDI electrode. In addition, PC–CDI's anode potential shift (0.06 V, from 0.87 V to 0.92 V) is significantly less than that of CDI (0.22 V, from 0.76 V to 0.98 V), which also supports the small PZC shift of PC–CDI. This is because, when PZC shift occurs, the potential window gradually shifts in the positive direction to form a closed loop for the CDI cell, thereby shifting both the anode potential and the cathode potential in the positive direction.

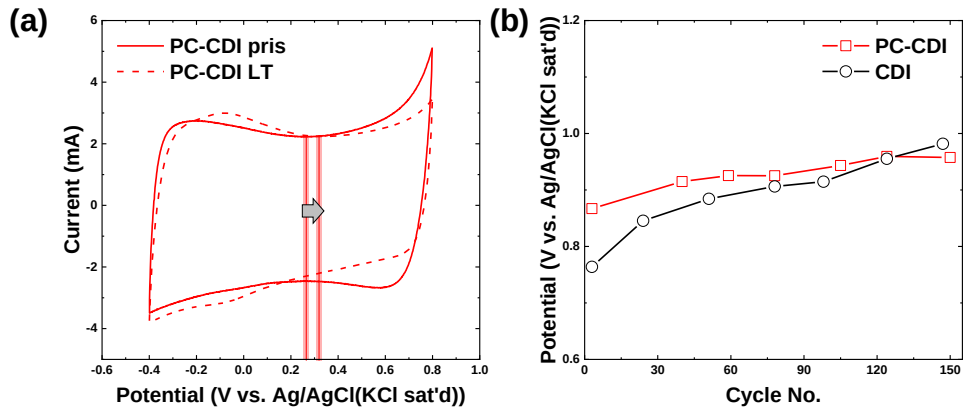

Figure 3-11 Cyclic voltammetry of (a) PC-electrode and (b) Anode potential changes for 150 cycles.

In order to investigate the reason for the low electrode oxidation of PC–CDI, the analysis of IEP coating morphology on the electrode was performed using SEM (Figure 3-12). Figure 3-12(a) shows the cross-section view of PC–electrode and Figure 3-12(b) shows the surface morphology of PC–CDI electrode at 3000 magnification. In Figure 3-12(a), IEP layer was not found on the outer surface of the electrode but it was observed that most of the surface of activated carbon particles were covered with IEP (Figure 3-12(b)). As shown in Figure 3-11(b), because the anode potentials of PC–CDI and CDI were maintained above 0.7 V (vs. Ag/AgCl (KCl sat'd)) for 150 cycles of operation, carbon oxidation reactions (Rxn (3)~(6) in section 2.2.2) should occur similarly in both systems due to their standard potential lower than anode potential. Nevertheless, decrease in SAC and PZC shift in PC–CDI was smaller than that in CDI. Therefore, the results can be interpreted that long-term stability can be improved by preventing the surface of activated carbon from being exposed to the water molecules.

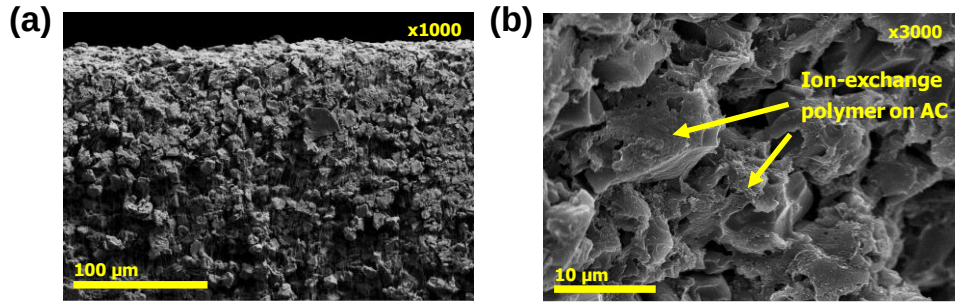

Figure 3-12 Cross section view of PC–CDI electrode with (a) 1000 magnification and (b) 3000 magnification.

3.4. Summary

In this chapter, PDA and IEP were coated on the surface of activated carbon as a means to prevent electrode oxidation, which causes the SAC reduction. As a result, it was possible to improve long term stability through the PDA coating, but the effect was relatively insignificant. The reason for this is that the low coating thickness of PDA was not able to completely prevent side reactions on the surface of activated carbon. In case of IEP coating, the long–term stability was greatly improved, which is considered to be due to the successful cover by IEP based on the thick coating on activated carbon, unlike PDA. Therefore, it was shown that IEP coating can improve the durability of CDI by successfully preventing electrode oxidation.

4. Effect of IEP layer thickness on long term stability

4.1. Background

In Chapter 3, it was shown that the long-term stability of the CDI can be improved by coating the surface of the activated carbon using PDA or IEPs. However, according to the literature, the improved long-term stability was also observed in MCDI which added an ion exchange membrane instead of coating activated carbon. In other words, even if activated carbon is exposed to water molecules to be oxidized, the long-term stability can be improved due to the certain role of the ion exchange membrane. Therefore, in this chapter, the role of IEP layer which exist on outer surface of the electrode was identified by coating the same IEP used in previous section with different thickness. To this end, the desalination performance and electrochemical properties of the IEP–coated oxidized electrodes, which means that IEP was coated on to pre-oxidized electrode. In addition, the electrical properties, desalination properties, and long-term stability were compared by controlling the thickness of the IEP layer.

4.2. Materials and method

4.2.1. Pre-oxidation of carbon electrode

The electrode was prepared in the same methods as described in Section 3.2.1, and then cut into a 50 mm diameter circle instead of 20 mm diameter.

The desalting operation was performed by assembling the prepared electrode and a spacer (200 μm thick) cut in a circular shape of 55 mm diameter. No modification was made to the electrodes. The cell used for pre-oxidation is a cell whose current collector is 50 mm in diameter (Figure 4-1), and the other form is the same as the cell having a diameter of 20 mm (Figure 3-2) used in Chapter 3. The influent was supplied with a NaCl 10 mM solution at a flow rate of about 10 mL min^{-1} to create the same environment of CDI. Note that the flow rate is increased to an appropriate level considering the size of the cell. The water that passed through the cell was applied to the influent pool again. 1.2 V was applied for 24 h using a battery cycler (WBCS3000, WonATech, Republic of Korea) for oxidation of the electrode, and then 0 V was applied for 10 min to regenerate the electrode. The effluent conductivity was monitored to confirm that the oxidation of the electrode occurs (conductivity meter, 3574-10C, HORIBA, Japan).

After the operation, the oxidized electrodes were collected and cut into three 20 mm diameter electrodes and their characteristics were evaluated (Figure 4-1). Three cut electrodes were used for the CDI and IEP–CCDI tests, respectively. In order to confirm the effects of electrode oxidation in various ways, four combinations were constructed with pristine electrode; pristine anode with pristine cathode (PA-PC), pristine anode with oxidized cathode

(PA-OC), oxidized anode with pristine cathode (OA-PC), and oxidized anode with oxidized cathode (OA-OC). For the evaluation for four combinations, short-term desalination test and electrochemical analyses (CV, EIS) were implemented.

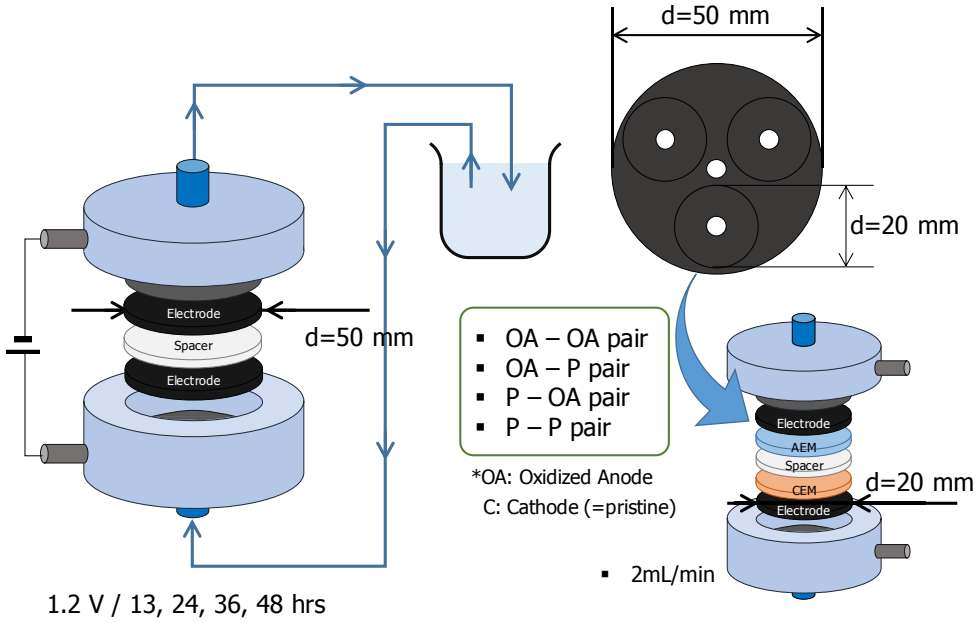

Figure 4-1 Schematic diagram for pre-oxidation of carbon electrode

4.2.2. Preparation of IEP-coated electrode

Overall sequences were the same with what is explained in section 3.2.2 except the polymer volume for coating. Approximately 3.5 mL and 5.5 mL of IEP was poured onto the carbon electrode for thickness of 30 μm and 100 μm, respectively. Also, drying time were more than 12 h for perfect drying. To distinguish the CDI system with the electrodes having different thickness, each system was named as IEP–CCDI (IEP-coated CDI) and the thickness of the IEP layer of electrode were followed (e.g. IEP–CCDI30, IEP–CCDI100).

4.2.3. Electrode characterization

The surface and cross section morphologies of carbon electrode and IEP-coated electrode were analyzed using field-emission scanning electron microscope (FE-SEM, SUPRA 55VP, Carl Zeiss, Germany). As electrochemical analyses, the cyclic voltammetry (CV) analysis and the electrochemical impedance spectroscopy (EIS) was carried out using a three-electrode cell. The cell was consisted of a carbon electrode or IEP-coated carbon electrode as a working electrode, a carbon electrode having about four times heavier mass as a counter electrode, and a reference electrode (Ag/AgCl (KCl sat'd)). The CV was conducted to measure the PZC in a range of – 0.4 ~ 0.6 V (vs. Ag/AgCl (KCl sat'd)) with 2 mV s^{-1} of scan rate using a

potentiostat (VersaSTAT 3, Princeton Applied Research, USA) for three cycles. The third cycle was used to find the PZC from the average value of the potential at the minimum current flowed during oxidation step and the maximum current flowed during reduction step (Yu et al., 2018).

4.3. Results and Discussion

4.3.1. MCDI test using pre-oxidized electrode

In order to confirm the degree of oxidation of the pre-oxidized electrode, first, a desalination test was conducted in a conventional CDI assembly. The electrical conductivity profile, shown as a straight line in Figure 4-2 (a), was measured prior to pre-oxidation and shows a typical CDI profile. However, the electrical conductivity of CDI using pre-oxidized electrode was rarely fluctuated (dotted line in Figure 4-2(a)) unlike that of CDI using pristine electrode. This tends to be similar to the electrical conductivity of the CDI's late cycles (Figure 4-2(b)), which was operated for 50 hours under normal operation. In other words, even if the 1.2V is applied in the pre-oxidation step without the regeneration step, the phenomena occurred the same with the normal CDI system operated for twice time. In Section 3.3.1, the electrode oxidation during CDI operation is shown to be constant while 1.2 V is applied. This phenomenon was observed the same in pre-oxidation experiment. As a result, the electrode obtained through pre-oxidation can represent the oxidized electrode in CDI operated for 50 hours.

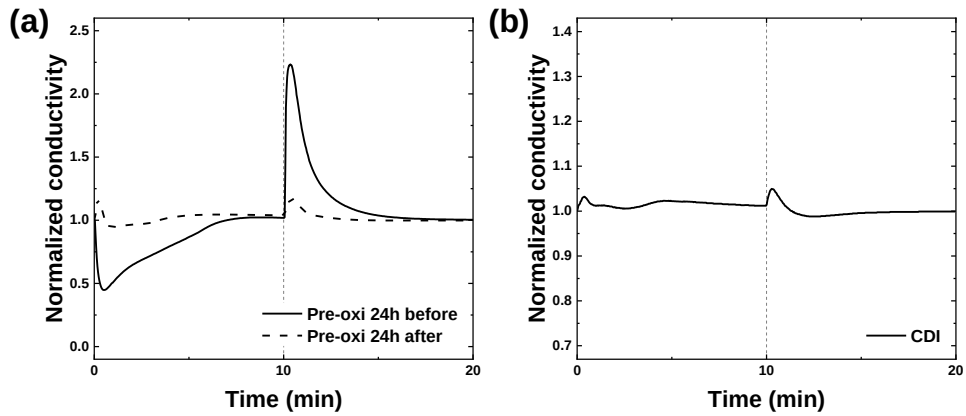

Figure 4-2 (a) Effluent conductivity profile of pre-oxidized electrode at initial cycle and after 24 h operation and (b) long-term operated electrode during 50 h

SS

Four combinations of CDI were constructed using pre-oxidized electrode and pristine electrode as anode or cathode. Among the terms used in Figure 4-3, 'P' means pristine electrode and 'O' means oxidized electrode prepared by pre-oxidation. The second letter of the name was anode (A) and cathode (C). For example, pristine electrode used as anode was named as PA and oxidized electrode used as a cathode was called as OC. Figure 4-3 (a) shows the change in electrical conductivity obtained by performing CDI operation for four combinations. The solid line indicates the use of the P electrode as an anode, the dashed line indicates the use of O electrode as the anode, the blue line indicates the use of the P electrode as the cathode, and the red line indicates the use of O electrode as the cathode.

In Figure 4-3(a), when the conductivity profile with same color is compared, the dotted line has a larger change than the solid line, and when the solid lines or the dotted lines are compared, the blue line has a larger change than the red line. This phenomenon is shown similarly in MCDI (Figure 4-3 (b)). In MCDI, however, the difference between the systems was significantly smaller than that of CDI.

For a more detailed comparison, the SAC calculated from the electrical conductivity was normalized to the case of using the PA-PC combination as shown in in Figure 4-3(c). The SAC values are listed in Table 4-1. There are

three major phenomena that can be interpreted in Figure 4-3 (c).

First, using O electrode as an anode (OA) greatly reduces performance. This is due to the PZC imbalance as described in Section 2.2.3 (Figure 4-4 (a)). In other words, the potential window must move in the positive direction to form a closed loop despite the PZC shift occurring at the anode. Then, the potential applied to the anode should be reduced because there is less potential window shift than the PZC shift. Therefore, the adsorption of ions was reduced.

Second, nevertheless, the rate of performance reduction in MCDI is significantly lower than that of CDI. If the reason for good long-term stability of MCDI is the only that the IEM prevents side reactions such as carbon oxidation, the SAC of MCDI would be significantly reduced like CDI when using pre-oxidized electrodes. However, the experimental results showed that such a decrease in SAC was small in MCDI. Thus, the role of the ion exchange membrane in MCDI is not only to prevent electrode oxidation but also to compensate the effect of electrode oxidation through another effect.

Third, the use of O electrode as the cathode (OC) increases SAC. This is observed more clearly in CDI. The increase in SAC is because the PZC shift, which causes a decrease in SAC, works in reverse. The reason why the SAC is high when the PZC shift works in reverse can be explained by using Figure

4-4. Figure 4-4 (a) is a scheme where the oxidized electrode is used as anode, as shown in Figure 2-9. As described above, the number of adsorbed ions, i.e., SAC, decreases by the reduction of the actual potential applied to the anode. On the other hand, Figure 4-4 (b) is a scheme where the oxidized electrode is used as cathode. In this case, the negative potential is applied to the PZC shifted electrode in the positive direction. Then, the actual potential applied to the electrode increases and consequently the SAC increases.

This researcher insisted that IEMs may compensate the effects of electrode oxidation based on the second phenomenon mentioned above. This effect can be explained by the well-known hypothesis that is widely accepted as the reason that MCDI performs better than CDI. First of all, there are two main reasons for MCDI to perform better than CDI (Biesheuvel and van der Wal, 2010,Biesheuvel et al., 2011,Zhao et al., 2012). As shown in Figure 4-5, one is that the co-ion, which is the ions having the opposite charge to the electrode, repulsion is inhibited due to ion selectivity of the ion exchange membrane, and the other is, nonetheless, that some co-ions inside the pores of the activated carbon are repulsed out of the pores to the inter-particle pores called macropore. In other words, the co-ions are concentrated in the macropore and additionally pulls counter-ion by the broken electroneutrality as the driving force. To be more specific, when Co-ion is stored in the macropore and

counter-ion enters the pores and is adsorbed, only the co-ion remains in the macropore, which collapses the electroneutrality of the electrolyte inside the macropore. Therefore, driving force is formed to adjust electroneutrality to neutral, and counter-ion is additionally move into macropore through the ion exchange membrane. This mechanism can be applied to CDI where PZC imbalance exists. In the regeneration stage where 0 V is applied, the co-ions adsorbed on the anode and the cathode (i.e., the cause of the inversion peak) are released out of the electrode when 1.2 V is applied. Note that these ions are the reasons of inversion peak of long-term operated CDI. The co-ions stay in macropore in MCDI while they are discharged with effluent in CDI. Then, in the same way, the co-ions will attract the counter-ion and the SAC increase by the number of ions participating in it.

Therefore, the coating material having ion exchange selectivity can be a solution to improve the long-term operation stability of CDI along with the electrode oxidation prevention phenomenon studied in Chapter 3. However, there is still a need to experimentally identify the effect of the thick polymer layer that acts like an ion exchange membrane in MCDI in the polymer coating CDI.

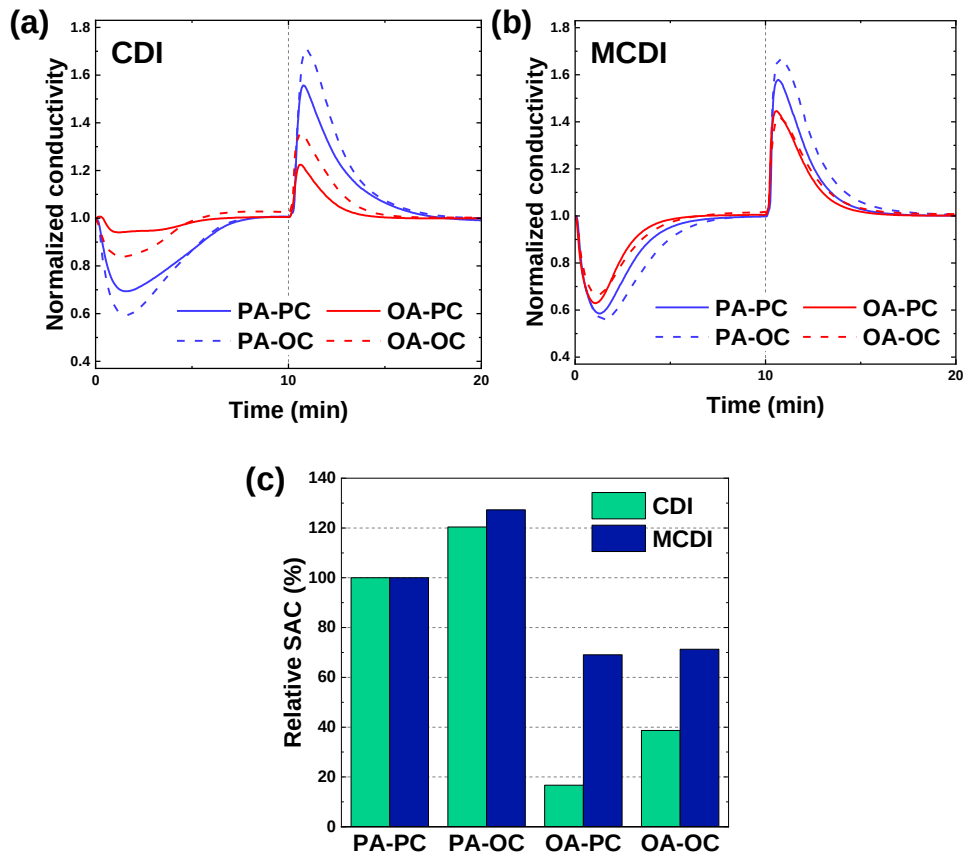

Figure 4-3 (a) Normalized conductivity profiles of 4 CDI assemblies, (b) that of 4 MCDI assemblies, and (c) relative SACs of CDI and MCDI based on the cell using both pristine electrode

Table 4-1 SAC values of CDI and MCDI for four pairs using pristine and pre-oxidized electrode

P – N	CDI [mg g^{-1}]	MCDI [mg g^{-1}]
PA – PC	11.4	13.3
PA – OC	13.7	16.9
OA – PC	1.9	9.2
OA – OC	4.4	9.5

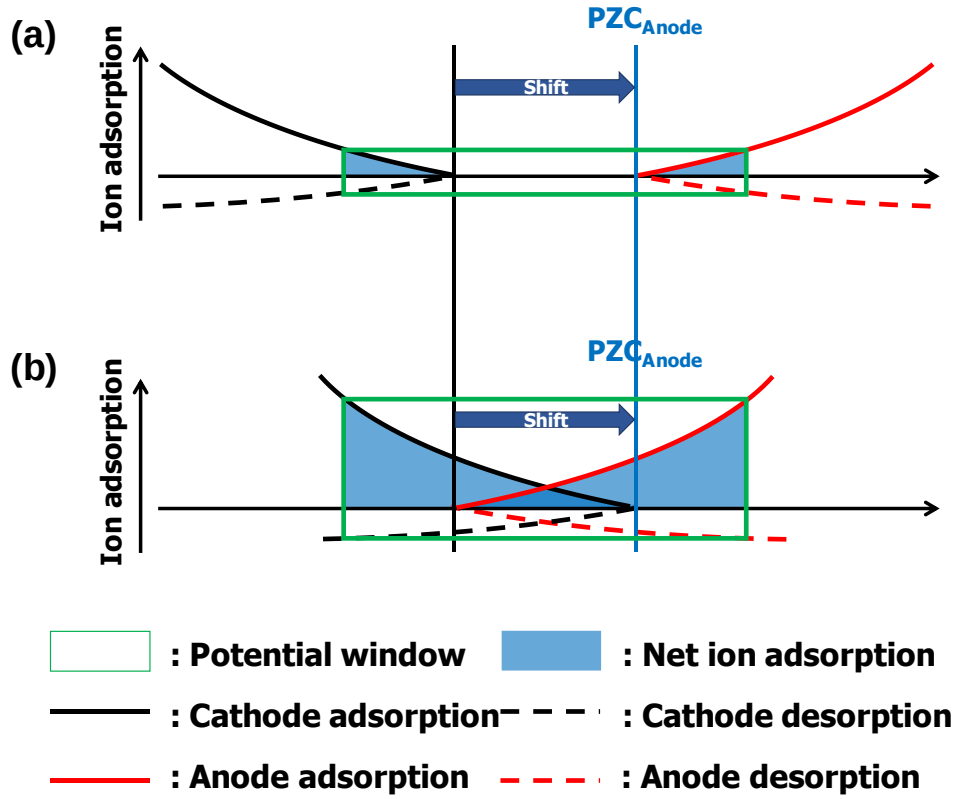

Figure 4-4 Schematic diagram about the effect of PZC shift to ion adsorption when oxidized electrode was used as (a) an anode and (b) a cathode.

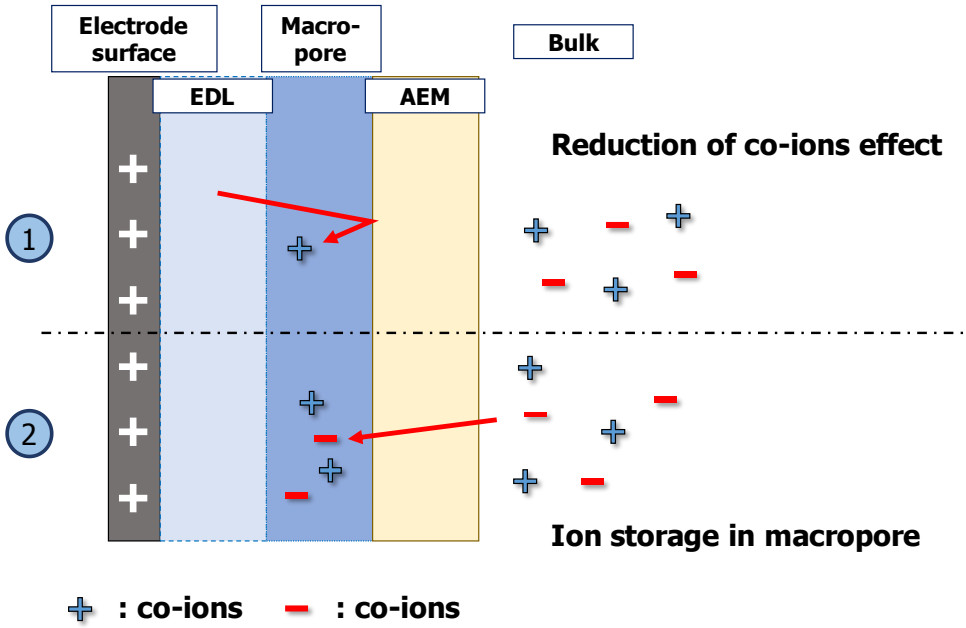

Figure 4-5 Schematic diagram for explaining the mechanisms of desalination performance improvement in MCDI compared to the performance in CDI

4.3.2. Long-term operation of IEP-CCDI with different thickness

First, SEM was conducted to check whether the electrode was well coated. As a result, as shown in Figure 4-6, the thicknesses of IEP layers were approximately 32 μm and 97 μm, respectively. In addition, the activated carbon of the electrode was covered with a polymer, so that the surface of the activated carbon was not smooth, as shown in Figure 3-12.

Figure 4-7(a) is a desalination test result using IEP coated electrode with IEP layer of various thickness to investigate the role of the ion exchange membrane. As summarized in Table 4-2, PC-CDI and IEP–CCDI30 showed similar SAC reduction of approximately 20% and 19%, respectively, while IEP–CCDI100 showed SAC reduction of only 12%, approximately. According to Yu et al., MCDI inserting only an IEM without a activated carbon surface coating using IEP showed dramatic improvement in long-term stability despite the carbon surface being exposed to water molecules (Yu et al., 2018). In this study, the thicker the IEP layer, the higher the initial SAC and the smaller the cycle. Therefore, the thick IEP layer is considered to have additional stability enhancement effect in addition to the effect of coating on the activated carbon.

The SAC value and the SAC reduction rate at the end of the operation are shown according to the thickness of the IEP layer (Figure 4-7 (b)). As can

be seen from the figure, as the thickness of the IEP layer became thicker, both the initial SAC value and the final SAC value increased, and the SAC reduction rate decreased.

At first, as the thickness of the IEP layer became thicker, the initial SAC was also increased due to the ion selectivity of the IEP. As has been widely reported in the literature, in CDI, the applied charges are wasted because of the co-ion repulsion effect, resulting in low charge efficiency. However, when ion exchange membrane is inserted in CDI to play a role as a charge barrier, charge efficiency as well as SAC can be improved due to the inhibition of co-ion repulsion effect (Jain et al., 2018,Kim and Choi, 2010b). This mechanism appears to be applied to IEP coated CDI. Therefore, thicker IEP layer appears to induce the increase of SAC because of the reinforced ability to inhibit the co-ion repulsion effect.

On the other hand, the reason why the final SAC value increased is because the initial SAC value increased and the SAC reduction decreased. If the thickness is increased, the resistance of the IEP layer increases, which may be because the degree of side reactions that may occur in the electrode is reduced. If the initial SAC is increased but the SAC reduction is large, the final SAC may appear relatively small. To support this discussion, the degree of side reaction can be examined by the PZC shift. As can be seen in Figure

4-8, the PZC of IEP–CCDI30 initially shifted by about 0.03 V from 0.2 V to 0.23 V, and the PZC of IEP–CCDI100 did not change at initial 0.26 V. Considering the results of PC–CDI (Figure 3-11), where the thickness of the ion exchange membrane can be assumed to be zero, it can be seen that the larger the thickness, the smaller the PZC shift, and the less side reaction.

In addition, it can be inferred from the characteristics of IEPs that the thicker the thickness, the lower the ion flux (Lopez et al., 2002). When the IEP layer is thicker, ions which should be repulsed out was more likely to be trapped inside the electrode due to the reduced ion flux, leading to an additional counter-ion adsorption. Therefore, it can be interpreted that the effect of compensation by IEP layer affected more to the SAC at later cycles.

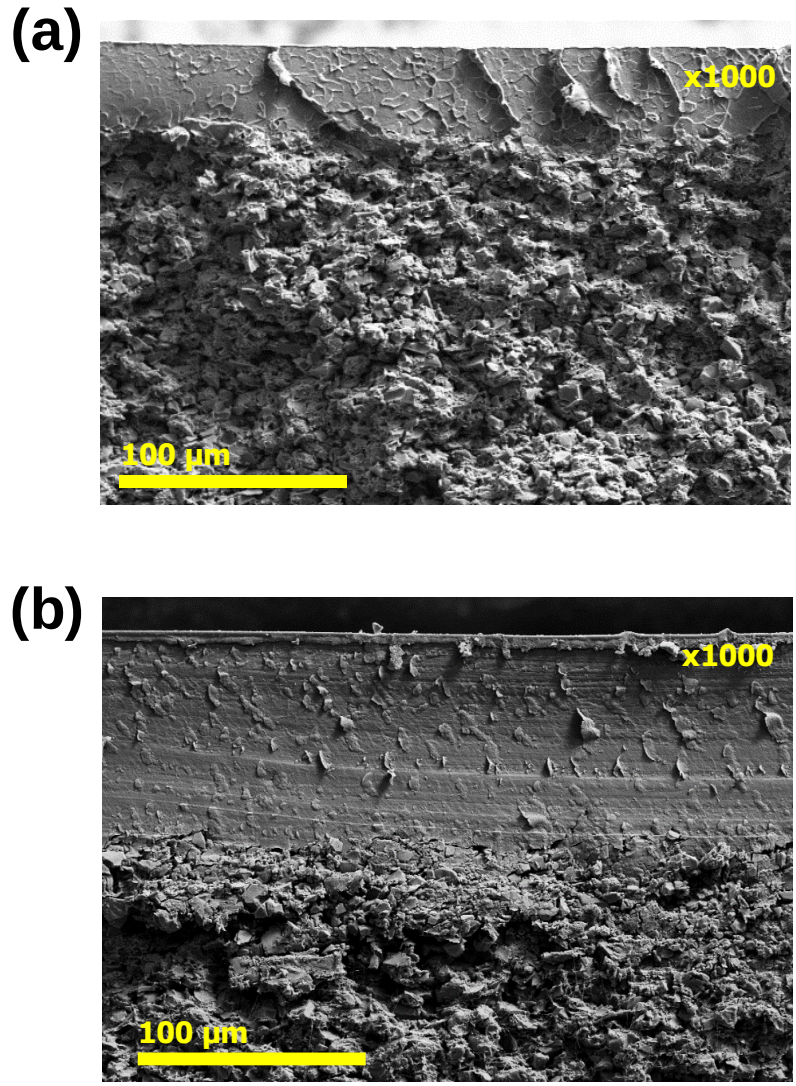

Figure 4-6 SEM images of (a) IEP–CCDI30 and (b) IEP–CCDI100

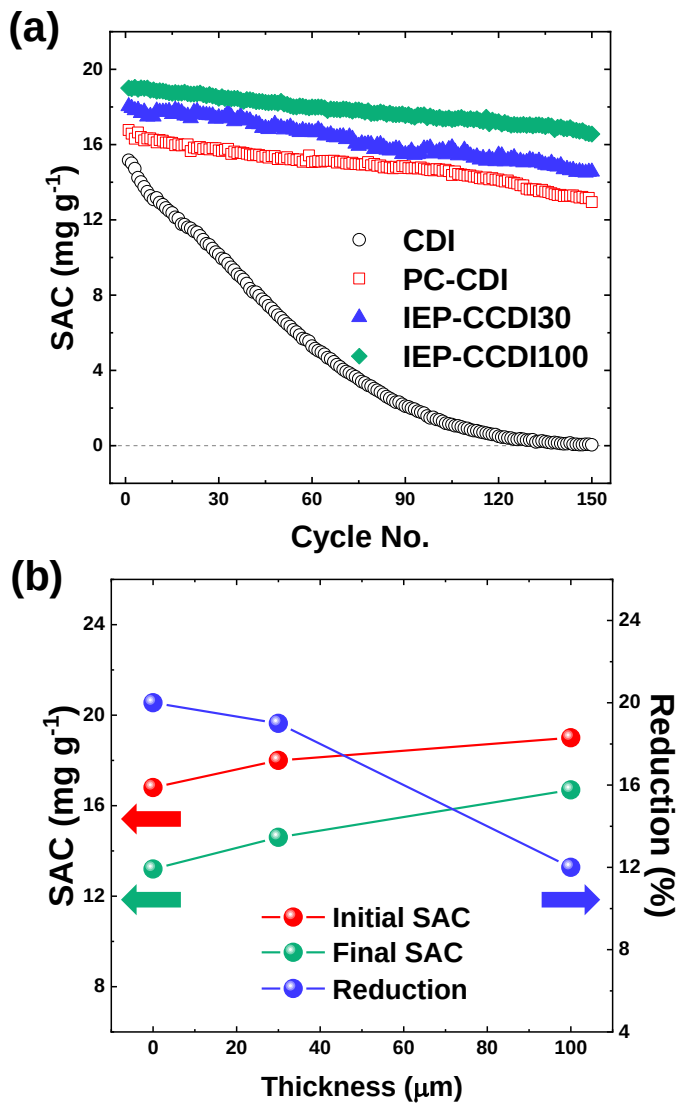

Figure 4-7 (a) Salt adsorption capacity (SAC) changes of thickness-controlled CCDI and CDI for 150 cycles and (b) the relationship between IEP-layer thickness and SAC, SAC reduction.

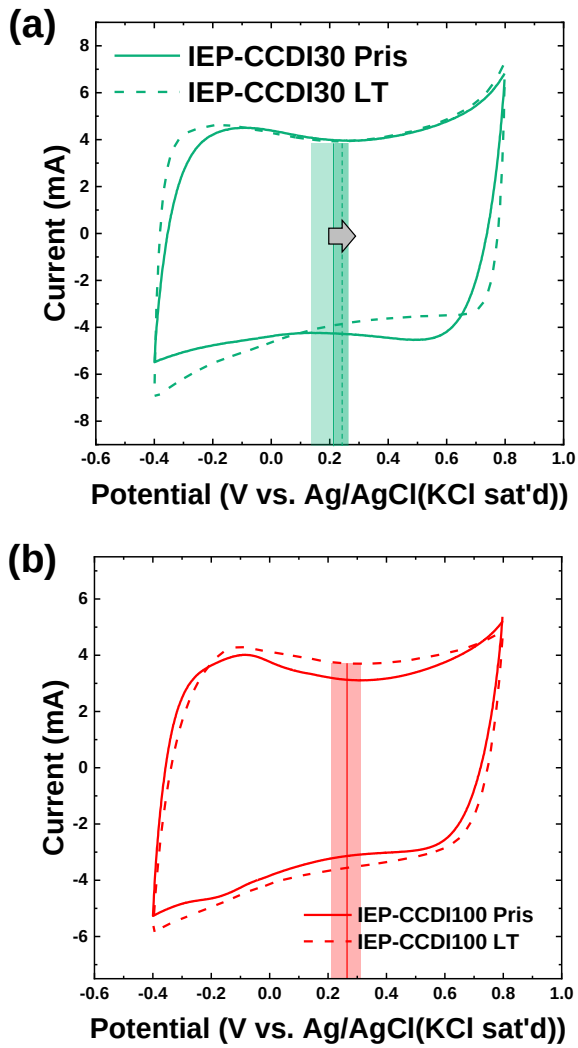

Figure 4-8 Cyclic voltammetry profile of (a) IEP–CCDI30 and (b) IEP–CCDI100 before and after long-term operation.

Figure 4-9 shows Nyquist plot ((a)) and the relationship between various resistances and IEP layer thickness ((b)) measured by EIS in order to examine the cause of the difference in stability and initial SAC of each system with different thickness of IEP layer. As can be seen in the figure, Nyquist plot of CDI using the electrode with thicker IEP layer was located at right side. Generally, Nyquist plot displays three representative resistance terms; electrical series resistance (ESR), charge transfer resistance (R_{ct}), and overall resistance ($R_{overall}$). ESR is the value of the x-intercept of the half-circle profile in the high frequency region and means the electrical resistance from the end of the cell to electrode-electrolyte interface. R_{ct} is obtained from the diameter of the half-circle and means the resistance of electron transparence when charge transfer reaction occurs at the electrode-electrolyte interface. At last, $R_{overall}$ is the average x-value of the points in a low frequency range that shows vertical increase (Bard and Faulkner, 2000,Funaki and Hikihara, 2008,Jang and Oh, 2010,Kim et al., 2012b,Liu et al., 2007b,Mei et al., 2018,Mei et al., 2017,Petek et al., 2016).

These three resistances were calculated from Nyquist plot and summarized in Table 4-2 and plotted versus IEP layer (Figure 4-9(b)). Among three resistances, R_{ct} is the most important in this research. It is because R_{ct} measured using EIS is a measure of how well various side reactions occur due

to that no faradaic reaction should occur, theoretically. As reported by several literatures in fuel cell area, carbon oxidation reactions could be observed as half circle in Nyquist plot (Bhandari et al., 2015,Boota et al., 2015,Liu et al., 2007a,Saeed et al., 2016,Zhao et al., 2015a,Zhao et al., 2015b). As a result, by focusing on Rct, it increased approximately 20% with addition of IEP layer of 30 μm and 80% with that of 100 μm. In consideration of this, it can be expected that the side reaction is the least at the IEP–CCDI100 since the resistance of the IEP–CCDI100 is the largest.

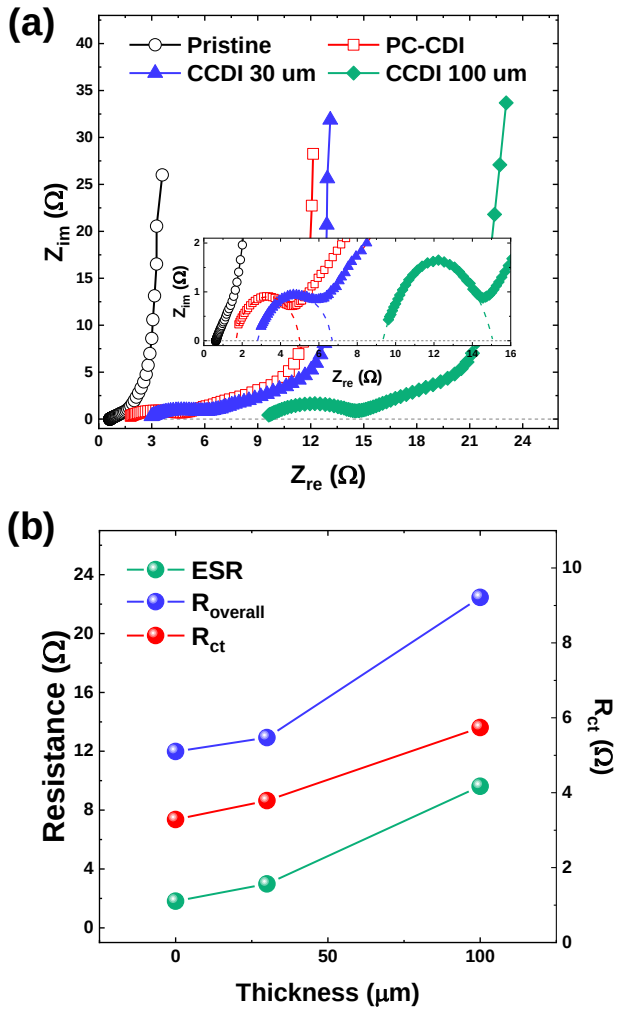

Figure 4-9 (a) Charge efficiency and (b) Nyquist plot of pristine and three IEP-coated electrodes with variation in thickness. An inset figure in (b) is enlarged impedance profile at high frequency range.

Table 4-2 SAC changes and resistances of pristine CDI and IEP-coated CDI

	Initial SAC ($mg\ g^{-1}$)	Final SAC ($mg\ g^{-1}$)	Reduction (%)	ESR (Ω)	R_{ct} (Ω)	$R_{overall}$ (Ω)
CDI	15.0	0.1	99	0.62	0.40	3.27
PC–CDI	16.8	13.2	20	1.81	1.64	11.98
IEP − CCDI 30 μm	18.0	14.6	19	2.98	1.89	12.93
IEP − CCDI 100 μm	19.0	16.7	12	9.62	2.87	22.46

Figure 4-10 shows the charge efficiency of each system. IEP–CCDI100 showed higher charge efficiency than PC-CDI or IEP–CCDI30 and PC–CDI and IEP–CCDI30 showed similar charge efficiency. This phenomenon is in good agreement with the trend of the impedance value in Figure 4-9(a) and Table 4-2. In the impedance results, the R_{ct} of the IEP–CCDI100 is the largest, and the R_{ct} of the IEP–CCDI30 and the PC–CDI were similar though that of the IEP–CCDI30 is slightly larger than PC–CDI. That is, in view of the fact that the charge efficiency is high in the system with a large R_{ct}, the R_{ct} may represent a side reaction, and the thicker the IEP layer, the less the side reaction. Therefore, when the electrode is coated with a thickness of 100 μm, better durability can be expected through fewer side reactions.

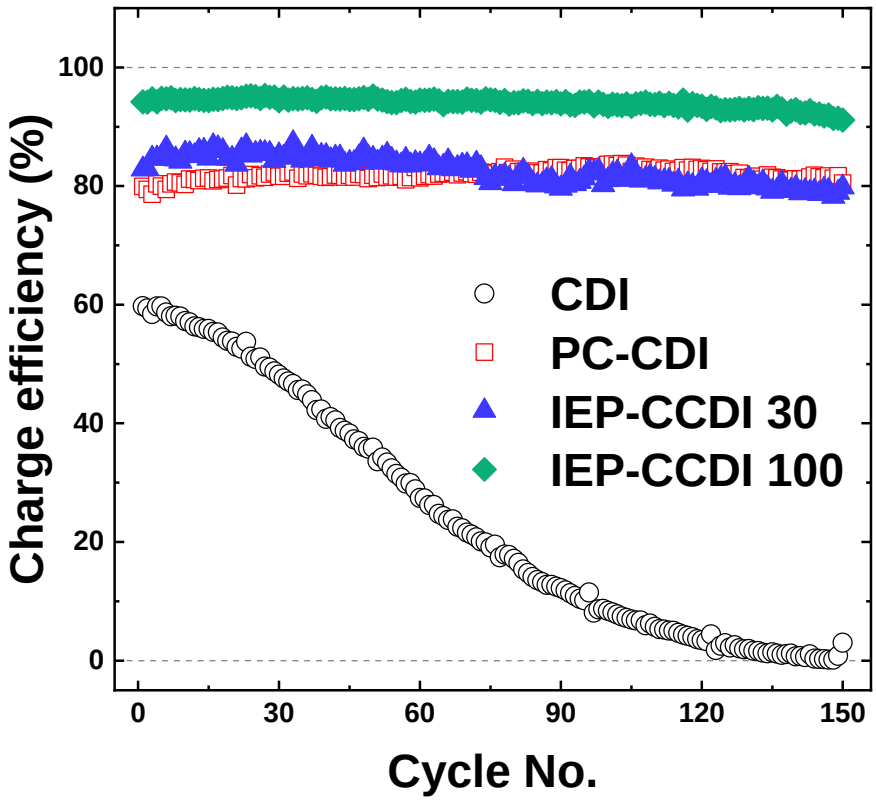

Figure 4-10 Charge efficiency of CDI, PC–CDI, IEP–CCDI30, and IEP–CCDI100.

However, it is not unconditionally good to increase the thickness of the IEP layer. This is because other resistances of IEP–CCDI 100 and 30 were relatively large compared to that of PC–CDI and CDI. The larger the ESR, the smaller the potential applied to the carbon electrode, so that the SAC can be reduced in consideration of the desalination principle of CDI which adsorbs ions as much as the applied potential. In addition, the larger the $R_{overall}$, the greater the amount of energy lost in moving ions from the influent to the inside of the electrode, which can also have a negative impact on energy efficiency. In addition, in the industrial aspect, the thick IEP layer may increase the volume of the entire module, thereby increasing the module cost. Therefore, considering the advantages of the thick IEP layer represented by R_{ct} and charge efficiency and the disadvantages represented by ESR, $R_{overall}$, and cost, it may be meaningful to find and apply the optimal thickness later.

5. Conclusion

In this dissertation, the effect of polymer coating on activated carbon electrodes for CDI on long term stability was investigated in terms of inhibition of carbon oxidation reaction and the compensation phenomena of IEP. At first, long term stability of polymer-coated CDI was improved by inhibiting carbon oxidation reactions due to the coverage of activated carbon surface by polydopamine (PDA) and IEP without any additional polymer layer on outer surface of the electrode. The main reason for poor long-term stability of CDI is due to that potential of zero charge (PZC) is changed by carbon oxidation reaction. PDA coating prevented this reaction from occurring as much as 10%. IEP coating was more effective than PDA, resulting in approximately 80% higher long-term stability, because the thicker coating layer than PDA coating inhibits carbon oxidation more successfully. Second, it was investigated that long-term stability of IEP coated CDI was much higher than that of CDI and the thicker IEP layer, the higher long-term stability. To investigate the cause, desalination performance of CDI using pre-oxidized electrode was evaluated. As a major result, IEP layer on outer surface of electrode played a role as the compensation barrier that utilizes repulsed co-ions by positive PZC shift that formation of IEP layer as well as a role that inhibits the carbon oxidation more based on larger charge transfer

resistance.

Therefore, it was found that the stability of CDI can be further improved by coating activated carbon using IEP and forming an IEP layer having an appropriate thickness. This study is meaningful in that it suggests a big direction to improve the stability required for the industrial application of CDI.

References

Álvarez-González, F.J.; Martín-Ramos, J.A.; Díaz, J.; Martínez, J.A.; Pernía, A.M. Energy-Recovery Optimization of an Experimental CDI Desalination System. *IEEE Transactions on Inducstrial Electronics* **2016**, *63*, 12

Aslan, M.; Zeiger, M.; Jackel, N.; Grobelsek, I.; Weingarth, D.; Presser, V. Improved capacitive deionization performance of mixed hydrophobic/hydrophilic activated carbon electrodes. *Journal of Physics: Condensed Matter* **2016**, *28*, 114003

Asquith, B.M.; Meier-Haack, J.; Ladewig, B.P. Cation exchange copolymer enhanced electrosorption. *Desalination* **2014**, *345*, 94-100

Asquith, B.M.; Meier-Haack, J.; Ladewig, B.P. Poly(arylene ether sulfone) copolymers as binders for capacitive deionization activated carbon electrodes. *Chemical Engineering Research and Design* **2015**, *104*, 81-91

Avasarala, B.; Moore, R.; Haldar, P. Surface oxidation of carbon supports due to potential cycling under PEM fuel cell conditions. *Electrochimica Acta* **2010**, *55*, 4765-4771

Avraham, E.; Noked, M.; Bouhadana, Y.; Soffer, A.; Aurbach, D. Limitations of charge efficiency in capacitive deionization processes III:

The behavior of surface oxidized activated carbon electrodes. *Electrochimica Acta* **2010**, *56*, 441-447

Bales, C.; Kovalsky, P.; Fletcher, J.; Waite, T.D. Low cost desalination of brackish groundwaters by Capacitive Deionization (CDI) – Implications for irrigated agriculture. *Desalination* **2019**, *453*, 37-53

Bard, A.J.; Faulkner, L.R. *Electrochemical Methods: Fundamentals and Applications*; Wiley: New York, 2000.

Bayram, E.; Ayranci, E. A systematic study on the changes in properties of an activated carbon cloth upon polarization. *Electrochimica Acta* **2011**, *56*, 2184-2189

Bhandari, N.; Dua, R.; Estevez, L.; Sahore, R.; Giannelis, E.P. A combined salt–hard templating approach for synthesis of multi-modal porous carbons used for probing the simultaneous effects of porosity and electrode engineering on EDLC performance. *Carbon* **2015**, *87*, 29-43

Biesheuvel, P.M.; van der Wal, A. Membrane capacitive deionization. *Journal of Membrane Science* **2010**, *346*, 256-262

Biesheuvel, P.M.; Zhao, R.; Porada, S.; van der Wal, A. Theory of membrane capacitive deionization including the effect of the electrode pore space. *Journal of Colloid and Interface Science* **2011**, *360*, 239-248

Boota, M.; Paranthaman, M.P.; Naskar, A.K.; Li, Y.; Akato, K.; Gogotsi, Y.

Waste Tire Derived Carbon-Polymer Composite Paper as Pseudocapacitive Electrode with Long Cycle Life. *ChemSusChem* **2015**, *8*, 3576-3581

Bouhadana, Y.; Avraham, E.; Noked, M.; Ben-Tzion, M.; Soffer, A.; Aurbach, D. Capacitive Deionization of NaCl Solutions at Non-Steady-State Conditions: Inversion Functionality of the Carbon Electrodes. *The Journal of Physical Chemistry C* **2011a**, *115*, 16567-16573

Bouhadana, Y.; Ben-Tzion, M.; Soffer, A.; Aurbach, D. A control system for operating and investigating reactors: The demonstration of parasitic reactions in the water desalination by capacitive de-ionization. *Desalination* **2011b**, *268*, 253-261

Che, X.; Wang, S.; Li, C.; Wang, G.; Li, C.; Wang, S.; Li, D.; Qiu, J. Inverted Capacitive Deionization with Highly Enhanced Stability Performance Utilizing Ionic Liquid-functionalized Carbon Electrodes. *ACS Sustainable Chemistry & Engineering* **2019**,

Choi, J.-H. Determination of the electrode potential causing Faradaic reactions in membrane capacitive deionization. *Desalination* **2014**, *347*, 224-229

Choi, J.H.; Yoon, D.J. A stable operation method for membrane capacitive deionization systems without electrode reactions at high cell potentials.

Water Research **2019**, *157*, 167-174

Choi, S.; Chang, B.; Kim, S.; Lee, J.; Yoon, J.; Choi, J.W. Battery Electrode Materials with Omnivalent Cation Storage for Fast and Charge-Efficient Ion Removal of Asymmetric Capacitive Deionization. *Advanced Functional Materials* **2018**,

Cohen, I.; Avraham, E.; Bouhadana, Y.; Soffer, A.; Aurbach, D. Long term stability of capacitive de-ionization processes for water desalination: The challenge of positive electrodes corrosion. *Electrochimica Acta* **2013**, *106*, 91-100

Cohen, I.; Avraham, E.; Bouhadana, Y.; Soffer, A.; Aurbach, D. The effect of the flow-regime, reversal of polarization, and oxygen on the long term stability in capacitive de-ionization processes. *Electrochimica Acta* **2015**, *153*, 106-114

Dlugolecki, P.; van der Wal, A. Energy recovery in membrane capacitive deionization. *Environmental Science & Technology* **2013**, *47*, 4904-4910

Evans, S.F.; Ivancevic, M.R.; Wilson, D.J.; Hood, Z.D.; Adhikari, S.P.; Naskar, A.K.; Tsouris, C.; Paranthaman, M.P. Carbon polyaniline capacitive deionization electrodes with stable cycle life. *Desalination* **2019**, *464*, 25-32

Funaki, T.; Hikihara, T. Characterization and Modeling of the Voltage

Dependency of Capacitance and Impedance Frequency Characteristics of Packed EDLCs. *IEEE Transactions on Power Electronics* **2008**, *23*, 1518-1525

Gao, X.; Omosebi, A.; Holubowitch, N.; Landon, J.; Liu, K. Capacitive Deionization Using Alternating Polarization: Effect of Surface Charge on Salt Removal. *Electrochimica Acta* **2017**, *233*, 249-255

Gao, X.; Omosebi, A.; Landon, J.; Liu, K. Dependence of the Capacitive Deionization Performance on Potential of Zero Charge Shifting of Carbon Xerogel Electrodes during Long-Term Operation. *Journal of the Electrochemical Society* **2014**, *161*, E159-E166

Gao, X.; Omosebi, A.; Landon, J.; Liu, K. Surface charge enhanced carbon electrodes for stable and efficient capacitive deionization using inverted adsorption–desorption behavior. *Energy & Environmental Science* **2015**, *8*, 897-909

Gurel, H.H.; Ciraci, S. Enhanced reduction of graphene oxide by means of charging and electric fields applied to hydroxyl groups. *Journal of Physics: Condensed Matter* **2013**, *25*, 435304

Hara, M.; Lee, M.; Liu, C.-H.; Chen, B.-H.; Yamashita, Y.; Uchida, M.; Uchida, H.; Watanabe, M. Electrochemical and Raman spectroscopic evaluation of Pt/graphitized carbon black catalyst durability for the

start/stop operating condition of polymer electrolyte fuel cells. *Electrochimica Acta* **2012**, *70*, 171-181

Hassanvand, A.; Chen, G.Q.; Webley, P.A.; Kentish, S.E. A comparison of multicomponent electrosorption in capacitive deionization and membrane capacitive deionization. *Water Research* **2017**, *131*, 100-109

He, D.; Wong, C.E.; Tang, W.; Kovalsky, P.; Waite, T.D. Faradaic Reactions in Water Desalination by Batch-Mode Capacitive Deionization. *Environmental Science & Technology* **2016**, *3*, 222-226

Hsieh, C.-T.; Chen, W.-Y.; Cheng, Y.-S. Influence of oxidation level on capacitance of electrochemical capacitors fabricated with carbon nanotube/carbon paper composites. *Electrochimica Acta* **2010**, *55*, 5294-5300

Hu, C.-C.; Hsieh, C.-F.; Chen, Y.-J.; Liu, C.-F. How to achieve the optimal performance of capacitive deionization and inverted-capacitive deionization. *Desalination* **2018**, *442*, 89-98

Jain, A.; Kim, J.; Owoseni, O.M.; Weathers, C.; Cana, D.; Zuo, K.; Walker, W.S.; Li, Q.; Verduzco, R. Aqueous-Processed, High-Capacity Electrodes for Membrane Capacitive Deionization. *Environmental Science & Technology* **2018**, *52*, 5859-5867

Jang, J.-H.; Oh, S.-M. Complex Capacitance Analysis of Impedance Data

and its Applications. *Journal of the Korean Electrochemical Society* **2010**, *13*, 223-234

Jeon, S.-i.; Park, H.-r.; Yeo, J.-g.; Yang, S.; Cho, C.H.; Han, M.H.; Kim, D.K. Desalination via a new membrane capacitive deionization process utilizing flow-electrodes. *Energy & Environmental Science* **2013**, *6*, 1471

Jeon, S.-i.; Yeo, J.-g.; Yang, S.; Choi, J.; Kim, D.K. Ion storage and energy recovery of a flow-electrode capacitive deionization process. *Journal of Materials Chemistry A* **2014**, *2*, 6378

Kang, J.; Kim, T.; Shin, H.; Lee, J.; Ha, J.-I.; Yoon, J. Direct energy recovery system for membrane capacitive deionization. *Desalination* **2016**, *398*, 144-150

Kim, C.; Kim, S.; Lee, J.; Kim, J.; Yoon, J. Capacitive and oxidant generating properties of black-colored TiO2 nanotube array fabricated by electrochemical self-doping. *ACS Applied Materials & Interfaces* **2015**, *7*, 7486-7491

Kim, C.; Lee, J.; Kim, S.; Yoon, J. TiO2 sol–gel spray method for carbon electrode fabrication to enhance desalination efficiency of capacitive deionization. *Desalination* **2014**, *342*, 70-74

Kim, J.-S.; Choi, J.-H. Fabrication and characterization of a carbon

electrode coated with cation-exchange polymer for the membrane capacitive deionization applications. *Journal of Membrane Science* **2010a**, *355*, 85-90

Kim, S.-J.; Choi, J.-H.; Kim, J.-H. Removal of acetic acid and sulfuric acid from biomass hydrolyzate using a lime addition–capacitive deionization (CDI) hybrid process. *Process Biochemistry* **2012a**, *47*, 2051-2057

Kim, S.; Kim, C.; Lee, J.; Kim, S.; Lee, J.; Kim, J.; Yoon, J. Hybrid Electrochemical Desalination System Combined with an Oxidation Process. *ACS Sustainable Chemistry & Engineering* **2018a**, *6*, 1620-1626

Kim, S.; Kim, J.; Kim, S.; Lee, J.; Yoon, J. Electrochemical lithium recovery and organic pollutant removal from industrial wastewater of a battery recycling plant. *Environmental Science: Water Research & Technology* **2018b**, *4*, 175-182

Kim, S.; Yu, G.; Kim, T.; Shin, K.; Yoon, J. Rapid bacterial detection with an interdigitated array electrode by electrochemical impedance spectroscopy. *Electrochimica Acta* **2012b**, *82*, 126-131

Kim, T.; Yu, J.; Kim, C.; Yoon, J. Hydrogen peroxide generation in flow-mode capacitive deionization. *Journal of Electroanalytical Chemistry* **2016**, *776*, 101-104

Kim, Y.-J.; Choi, J.-H. Enhanced desalination efficiency in capacitive deionization with an ion-selective membrane. *Separation and Purification Technology* **2010b**, *71*, 70-75

Kim, Y.-J.; Kim, J.-H.; Choi, J.-H. Selective removal of nitrate ions by controlling the applied current in membrane capacitive deionization (MCDI). *Journal of Membrane Science* **2013**, *429*, 52-57

Kim, Y.J.; Choi, J.H. Improvement of desalination efficiency in capacitive deionization using a carbon electrode coated with an ion-exchange polymer. *Water Research* **2010c**, *44*, 990-996

Kim, Y.J.; Choi, J.H. Selective removal of nitrate ion using a novel composite carbon electrode in capacitive deionization. *Water Research* **2012**, *46*, 6033-6039

Lado, J.J.; Pérez-Roa, R.E.; Wouters, J.J.; Tejedor-Tejedor, M.I.; Federspill, C.; Anderson, M.A. Continuous cycling of an asymmetric capacitive deionization system: An evaluation of the electrode performance and stability. *Journal of Environmental Chemical Engineering* **2015**, *3*, 2358-2367

Lee, H.; Dellatore, S.M.; Miller, W.M.; Messersmith, P.B. Mussel-inspired surface chemistry for multifunctional coatings. *Science* **2007**, *318*, 426-430

Lee, J.-B.; Park, K.-K.; Eum, H.-M.; Lee, C.-W. Desalination of a thermal power plant wastewater by membrane capacitive deionization. *Desalination* **2006**, *196*, 125-134

Lee, J.-H.; Bae, W.-S.; Choi, J.-H. Electrode reactions and adsorption/desorption performance related to the applied potential in a capacitive deionization process. *Desalination* **2010**, *258*, 159-163

Lee, J.-H.; Choi, J.-H. The production of ultrapure water by membrane capacitive deionization (MCDI) technology. *Journal of Membrane Science* **2012**, *409-410*, 251-256

Lee, J.; Kim, S.; Kim, C.; Yoon, J. Hybrid capacitive deionization to enhance the desalination performance of capacitive techniques. *Energy & Environmental Science* **2014**, *7*, 3683-3689

Lee, J.Y.; Seo, S.J.; Yun, S.H.; Moon, S.H. Preparation of ion exchanger layered electrodes for advanced membrane capacitive deionization (MCDI). *Water Research* **2011**, *45*, 5375-5380

Li, H.; Pan, L.; Lu, T.; Zhan, Y.; Nie, C.; Sun, Z. A comparative study on electrosorptive behavior of carbon nanotubes and graphene for capacitive deionization. *Journal of Electroanalytical Chemistry* **2011**, *653*, 40-44

Li, N.; An, J.K.; Wang, X.; Wang, H.M.; Lu, L.; Ren, Z.Y.J.S. Resin-

enhanced rolling activated carbon electrode for efficient capacitive deionization. *Desalination* **2017**, *419*, 20-28

Liu, C.-L.; Dong, W.-S.; Cao, G.-P.; Song, J.-R.; Liu, L.; Yang, Y.-S. Influence of KOH followed by oxidation pretreatment on the electrochemical performance of phenolic based activated carbon fibers. *Journal of Electroanalytical Chemistry* **2007a**, *611*, 225-231

Liu, X.-m.; Zhang, R.; Zhan, L.; Long, D.-h.; Qiao, W.-m.; Yang, J.-h.; Ling, L.-c. Impedance of carbon aerogel/activated carbon composites as electrodes of electrochemical capacitors in aprotic electrolyte. *New Carbon Materials* **2007b**, *22*, 153-158

Liu, Y.; Pan, L.; Xu, X.; Lu, T.; Sun, Z.; Chua, D.H.C. Enhanced desalination efficiency in modified membrane capacitive deionization by introducing ion-exchange polymers in carbon nanotubes electrodes. *Electrochimica Acta* **2014**, *130*, 619-624

Lopez, M.; Kipling, B.; Yeager, H.L. Ionic diffusion and selectivity of a cation exchange membrane in nonaqueous solvents. *Analytical Chemistry* **2002**, *49*, 629-632

Ma, D.; Cai, Y.; Wang, Y.; Xu, S.; Wang, J.; Khan, M.U. Grafting the Charged Functional Groups on Carbon Nanotubes for Improving the Efficiency and Stability of Capacitive Deionization Process. *ACS*

Applied Materials & Interfaces **2019a**, *11*, 17617-17628

Ma, J.; Liang, P.; Sun, X.; Zhang, H.; Bian, Y.; Yang, F.; Bai, J.; Gong, Q.; Huang, X. Energy recovery from the flow-electrode capacitive deionization. *Journal of Power Sources* **2019b**, *421*, 50-55

Ma, J.; Zhang, Y.; Collins, R.N.; Tsarev, S.; Aoyagi, N.; Kinsela, A.S.; Jones, A.M.; Waite, T.D. Flow-Electrode CDI Removes the Uncharged Ca-UO2-CO3 Ternary Complex from Brackish Potable Groundwater: Complex Dissociation, Transport, and Sorption. *Environmental Science and Technology* **2019c**, *53*, 2739-2747

Maass, S.; Finsterwalder, F.; Frank, G.; Hartmann, R.; Merten, C. Carbon support oxidation in PEM fuel cell cathodes. *Journal of Power Sources* **2008**, *176*, 444-451

Mei, B.-A.; Lau, J.; Lin, T.; Tolbert, S.H.; Dunn, B.S.; Pilon, L. Physical Interpretations of Electrochemical Impedance Spectroscopy (EIS) of Redox Active Electrodes for Electrical Energy Storage. *The Journal of Physical Chemistry C* **2018**,

Mei, B.-A.; Munteshari, O.; Lau, J.; Dunn, B.; Pilon, L. Physical Interpretations of Nyquist Plots for EDLC Electrodes and Devices. *The Journal of Physical Chemistry C* **2017**, *122*, 194-206

Nugrahenny, A.T.U.; Kim, J.; Lim, S.; Jung, D.-H. Development of high

performance cell structure for capacitive deionization using membrane polymer-coated electrode. In Proceedings of CISAK.

Omosebi, A.; Gao, X.; Holubowitch, N.; Li, Z.; Landon, J.; Liu, K. Anion Exchange Membrane Capacitive Deionization Cells. *Journal of the Electrochemical Society* **2017**, *164*, E242-E247

Omosebi, A.; Gao, X.; Landon, J.; Liu, K. Asymmetric electrode configuration for enhanced membrane capacitive deionization. *ACS Applied Materials & Interfaces* **2014**, *6*, 12640-12649

Oyarzun, D.I.; Hemmatifar, A.; Palko, J.W.; Stadermann, M.; Santiago, J.G. Adsorption and capacitive regeneration of nitrate using inverted capacitive deionization with surfactant functionalized carbon electrodes. *Separation and Purification Technology* **2018**, *194*, 410-415

Park, H.-r.; Choi, J.; Yang, S.; Kwak, S.J.; Jeon, S.-i.; Han, M.H.; Kim, D.K. Surface-modified spherical activated carbon for high carbon loading and its desalting performance in flow-electrode capacitive deionization. *RSC Advances* **2016**, *6*, 69720-69727

Park, Y.-C.; Kakinuma, K.; Uchida, M.; Tryk, D.A.; Kamino, T.; Uchida, H.; Watanabe, M. Investigation of the corrosion of carbon supports in polymer electrolyte fuel cells using simulated start-up/shutdown cycling. *Electrochimica Acta* **2013**, *91*, 195-207

Pernía, A.M.; Prieto, M.J.; Martín-Ramos, J.A.; Villegas, P.J.; Álvarez-González, F.J. Energy Recovery in Capacitive Deionization Technology. In *Desalination and Water Treatment*, 2018.

Petek, T.J.; Hoyt, N.C.; Savinell, R.F.; Wainright, J.S. Characterizing Slurry Electrodes Using Electrochemical Impedance Spectroscopy. *Journal of the Electrochemical Society* **2016**, *163*, A5001-A5009

Qin, M.; Deshmukh, A.; Epsztein, R.; Patel, S.K.; Owoseni, O.M.; Walker, W.S.; Elimelech, M. Comparison of energy consumption in desalination by capacitive deionization and reverse osmosis. *Desalination* **2019**, *455*, 100-114

Ryu, J.H.; Messersmith, P.B.; Lee, H. Polydopamine Surface Chemistry: A Decade of Discovery. *ACS Applied Materials & Interfaces* **2018**, *10*, 7523-7540

Saeed, A.A.; Singh, B.; Nooredeen Abbas, M.; Dempsey, E. Evaluation of Bismuth Modified Carbon Thread Electrode for Simultaneous and Highly Sensitive Cd (II) and Pb (II) Determination. *Electroanalysis* **2016**, *28*, 2205-2213

Srimuk, P.; Ries, L.; Zeiger, M.; Fleischmann, S.; Jäckel, N.; Tolosa, A.; Krüner, B.; Aslan, M.; Presser, V. High performance stability of titania decorated carbon for desalination with capacitive deionization in

oxygenated water. *RSC Advances* **2016**, *6*, 106081-106089

Suss, M.E.; Baumann, T.F.; Bourcier, W.L.; Spadaccini, C.M.; Rose, K.A.; Santiago, J.G.; Stadermann, M. Capacitive desalination with flow-through electrodes. *Energy & Environmental Science* **2012**, *5*, 9511

Suss, M.E.; Porada, S.; Sun, X.; Biesheuvel, P.M.; Yoon, J.; Presser, V. Water desalination via capacitive deionization: what is it and what can we expect from it? *Energy & Environmental Science* **2015**, *8*, 2296-2319

Tang, W.; He, D.; Zhang, C.; Kovalsky, P.; Waite, T.D. Comparison of Faradaic reactions in capacitive deionization (CDI) and membrane capacitive deionization (MCDI) water treatment processes. *Water Research* **2017a**, *120*, 229-237

Tang, W.; He, D.; Zhang, C.; Waite, T.D. Optimization of sulfate removal from brackish water by membrane capacitive deionization (MCDI). *Water Research* **2017b**, *121*, 302-310

Vujković, M.; Bajuk-Bogdanović, D.; Matović, L.; Stojmenović, M.; Mentus, S. Mild electrochemical oxidation of zeolite templated carbon in acidic solutions, as a way to boost its charge storage properties in alkaline solutions. *Carbon* **2018**, *138*, 369-378

Xie, Z.; Cheng, J.; Yan, J.; Cai, W.; Nie, P.; Chan, H.T.H.; Liu, J. Polydopamine Modified Activated Carbon for Capacitive Desalination.

Journal of the Electrochemical Society **2017**, *164*, A2636-A2643

Yeo, J.-H.; Choi, J.-H. Enhancement of nitrate removal from a solution of mixed nitrate, chloride and sulfate ions using a nitrate-selective carbon electrode. *Desalination* **2013**, *320*, 10-16

Yi, Y.; Weinberg, G.; Prenzel, M.; Greiner, M.; Heumann, S.; Becker, S.; Schlögl, R. Electrochemical corrosion of a glassy carbon electrode. *Catalysis Today* **2017**, *295*, 32-40

Yoon, D.J.; Choi, J.H. A new standard metric describing the adsorption capacity of carbon electrode used in membrane capacitive deionization. *Water Research* **2018**, *148*, 126-132

Yoon, H.; Lee, J.; Kim, S.; Yoon, J. Electrochemical sodium ion impurity removal system for producing high purity KCl. *Hydrometallurgy* **2018**, *175*, 354-358

Yoon, H.; Lee, J.; Kim, S.; Yoon, J. Review of concepts and applications of electrochemical ion separation (EIONS) process. *Separation and Purification Technology* **2019**, *215*, 190-207

Yu, J. Analysis of Faradaic REaction and Its Effect on Desalination Performance in Capacitive Deionization. Seoul National University, Seoul National University, 2017.

Yu, J.; Jo, K.; Kim, T.; Lee, J.; Yoon, J. Temporal and spatial distribution

of pH in flow-mode capacitive deionization and membrane capacitive deionization. *Desalination* **2018**, *439*, 188-195

Zhang, C.; He, D.; Ma, J.; Tang, W.; Waite, T.D. Faradaic reactions in capacitive deionization (CDI) - problems and possibilities: A review. *Water Research* **2018**, *128*, 314-330

Zhang, C.; He, D.; Ma, J.; Tang, W.; Waite, T.D. Comparison of faradaic reactions in flow-through and flow-by capacitive deionization (CDI) systems. *Electrochimica Acta* **2019**, *299*, 727-735

Zhao, R.; Biesheuvel, P.M.; Miedema, H.; Bruning, H.; van der Wal, A. Charge Efficiency: A Functional Tool to Probe the Double-Layer Structure Inside of Porous Electrodes and Application in the Modeling of Capacitive Deionization. *The Journal of Physical Chemistry Letters* **2009**, *1*, 205-210

Zhao, R.; Biesheuvel, P.M.; van der Wal, A. Energy consumption and constant current operation in membrane capacitive deionization. *Energy & Environmental Science* **2012**, *5*, 9520

Zhao, S.; Li, Y.; Yin, H.; Liu, Z.; Luan, E.; Zhao, F.; Tang, Z.; Liu, S. Three-dimensional graphene/Pt nanoparticle composites as freestanding anode for enhancing performance of microbial fuel cells. *Science Advances* **2015a**, *1*, e1500372

Zhao, Z.; Zhang, M.; Li, Y.; Cheng, S.; Chen, X.; Wang, J. Evaluation of Electrochemically Reduced Gold Nanoparticle—Graphene Nanocomposites for the Determination of Dopamine. *Analytical Letters* **2015b**, *48*, 1437-1453

국문 초록

축전식 탈염 공정(Capacitive deionization, CDI)는 일상 생활에 깨끗한 물을 충분히 공급하기 위한 다양한 탈염 기술 중 하나이다. 축전식 탈염 공정은 다른 담수화 기술에 비해 에너지 소비, 물 회수율 및 환경 친화성 측면에서 장점을 갖는 담수화 기술로 주목을 받고 있다. 그러나, 장기 운전 시 탈염 성능의 저하로 인해 어려움을 겪고 있으며 이는 실제 현장에 적용하기 위해서는 꼭 해결해야 할, 매우 중요한 문제이다. 탈염 성능 저하의 주요 원인인 탄소 산화 및 그로 인한 표면 변화를 억제함으로써 문제를 극복할 수 있지만, 이러한 목적을 구현하거나 그 원리에 대해 규명한 연구가 현재까지는 부족한 실정이다.

이 논문에서는 CDI용 활성탄 전극에 폴리도파민과 이온교환고분자를 코팅하고, 장기 운전 시 성능이 어떻게 변화하는지를 조사하였다. 먼저, 이온 교환 고분자가 전극의 산화를 실제로 방지하는지 여부를 조사하기 위해 전극의 바깥쪽 표면에 어떠한 고분자층도 없도록 활성탄에 폴리 도파민 또는 이온 교환 고분자를 코팅하였다. 이 전극을 사

용하여 CDI의 장기 운전 시 탈염 성능 변화를 추적한 결과, 폴리도파민 코팅 시 약 10 %만큼의 탈염 성능 감소 방지 효과가 관찰되었고, 이온 교환 고분자 코팅 시 80%의 성능이 50시간 후에도 유지됨으로써 폴리도파민보다 효과적이라는 결과를 얻었다. 이러한 장기 운전 내구성의 향상은 폴리도파민 및 이온교환고분자의 코팅이 탄소의 산화를 성공적으로 억제했기 때문이다.

둘째, 이온 교환 중합체 층의 역할을 조사하기 위해, 미리 산화시킨 전극에 대하여 CDI, MCDI 테스트를 진행하였고, 다양한 두께 (30 μm, 100 μm)로 이온교환고분자를 코팅한 전극을 사용하여 CDI의 장기 안정성을 측정하고 비교했다. 그 결과, 24 시간 동안 사전 산화된 전극을 사용한 MCDI는 CDI에 비해 성능 감소가 덜 나타났다. 이는 이온 교환막이 단순히 부반응을 줄이는 역할뿐만 아니라 탄소 산화에 의한 영전하 전위 영향을 상쇄하는 역할도 수행한다는 것을 의미한다. 이 효과는 다른 두께로 이온교환고분자를 코팅한 전극을 사용한 CDI 테스트를 통해 보다 체계적으로 조사되었다. 그 결과, 두께가 두꺼울

수록 더 우수한 장기 안정성을 나타냈다. 두꺼운 이온교환고분자는 셀의 전기적 저항을 키움에도 불구하고 더 좋은 장기 안정성 및 더 좋은 탈염 성능이 나타난 이유는 MCDI 실험에서 확인된 바와 같이 양의 방향으로 이동한 영전하 전위에 의해 밀려난 동전하 이온이 버려지지 않고 반대전하 이온을 끌어오는 데 쓰이도록 하기 때문이다. 그와 동시에 탄소 산화를 더욱 억제하는 역할도 더 강하게 수행하기 때문에 뛰어난 장기 운전 내구성을 보임을 확인하였다.

따라서, 다양한 고분자를 사용하여 활성탄을 코팅하고 적절한 두께를 갖는 이온교환고분자층을 형성함으로써 CDI의 안정성을 추가로 개선할 수 있을 것으로 기대된다. 그러므로 이 연구는 CDI의 실제 적용에 필요한 수준의 안정성을 확보하기 위한 큰 방향을 제시한다는 점에서 의미가 있다고 사료된다.